State of stress in central and eastern North American seismic zones

Stephane Mazzotti[1] and John Townend[2]

[1]GEOLOGICAL SURVEY OF CANADA, NATURAL RESOURCES CANADA, P.O. BOX 6000, SIDNEY, BC V8L 4B2, CANADA *AND* SCHOOL OF EARTH AND OCEAN SCIENCES, UNIVERSITY OF VICTORIA, PO BOX 3065 STN CSC, VICTORIA, BC V8W 3V6, CANADA

[2]SCHOOL OF GEOGRAPHY, ENVIRONMENT, AND EARTH SCIENCES, VICTORIA UNIVERSITY OF WELLINGTON, P.O. BOX 600, WELLINGTON 6140, NEW ZEALAND

ABSTRACT

We use a Bayesian analysis to determine the state of stress from focal mechanisms in ten seismic zones in central and eastern North America and compare it with regional stress inferred from borehole measurements. Comparisons of the seismologically determined azimuth of the maximum horizontal compressive stress (S_{HS}) with that determined from boreholes (S_{HB}) exhibit a bimodal pattern: In four zones, the S_{HS} and regional S_{HB} orientations are closely parallel, whereas in the Charlevoix, Lower St. Lawrence, and Central Virginia zones, the S_{HS} azimuth shows a statistically significant 30°–50° clockwise rotation relative to the regional S_{HB} azimuth. This pattern is exemplified by the northwest and southeast seismicity clusters in Charlevoix, which yield S_{HS} orientations strictly parallel and strongly oblique, respectively, to the regional S_{HB} trend. Similar ~30° clockwise rotations are found for the North Appalachian zone and for the 2003 Bardwell earthquake sequence north of the New Madrid zone. The S_{HB}/S_{HS} rotations occur over 20–100 km in each seismic zone, but they are observed in zones separated by distances of up to 1500 km. A possible mechanism for the stress rotations may be the interaction between a long-wavelength stress perturbation source, such as postglacial rebound, and local stress concentrators, such as low-friction faults. The latter would allow low-magnitude (<10 MPa) postglacial rebound stresses to locally perturb the preexisting stress field in some seismic zones, whereas postglacial rebound stresses have little effect on the intraplate state of stress in general.

LITHOSPHERE; v. 2; no. 2; p. 76–83, Data Repository 2010020. doi: 10.1130/L65.1

INTRODUCTION

As in most continental intraplate regions, stress orientations in central and eastern North America are broadly homogeneous and consistent over 1000–5000 km spatial scales (e.g., Zoback and Zoback, 1980, 1991; Zoback, 1992a). East of the Cordillera deformation front, the main characteristic of the tectonic stress field is a NE-SW axis of maximum horizontal compressive stress (S_H), which is commonly attributed to far-field plate-boundary forces, and in particular to Mid-Atlantic Ridge push (Zoback, 1992a; Richardson, 1992). In a case study of 32 eastern North American earthquakes, Zoback (1992b) noted that most focal mechanisms were compatible with the regional stress field inferred from borehole data. However, five mechanisms suggested local stress perturbations, and two other events implied atypical frictional conditions (e.g., superlithostatic pore-fluid pressure).

The spatial distribution of earthquakes in central and eastern North America is largely associated with late Proterozoic Iapetus Rift structures (e.g., Adams and Basham, 1991; Johnston et al., 1994). As shown in Figure 1, the main concentrations of both small and large earthquakes lie along the rifted margin itself or failed rift arms. The Iapetus structures are typically reactivated under the present-day stress

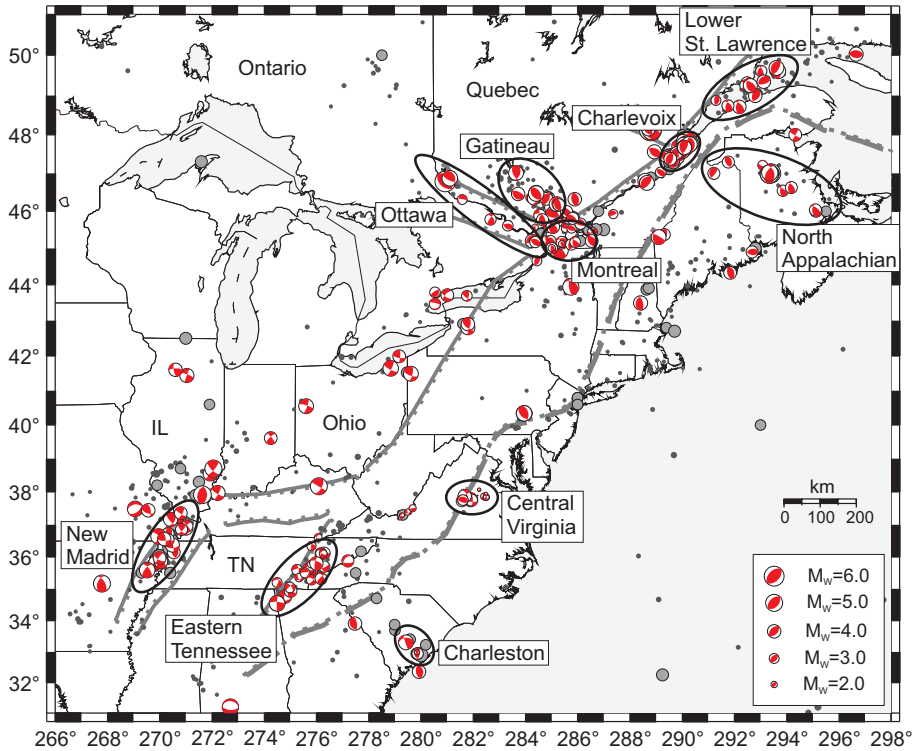

Figure 1. Central and eastern North America seismicity and Iapetus Rift structures. Dark- and light-gray dots show magnitude M ≥ 3 and M ≥ 5 earthquakes since 1973 (Geological Survey of Canada and U.S. Geological Survey catalogs). Focal mechanism (red) sources are given in the supplementary material (see text footnote 1). Thick gray barbed lines indicate the Iapetus rifted margin and failed rifts. The ten seismic zones discussed in the text are shown by solid ellipses.

field as thrust or strike-slip faults. Aside from this first-order correlation, rather little is known about the geological and geophysical conditions generating intraplate earthquakes and the associated hazard (cf. Stein and Mazzotti, 2007, and references therein). Thus, characterization of the regional stress field and local state of stress is essential for improving our understanding of the source of intraplate seismicity and better quantifying seismic hazard.

In this study, we analyze a newly compiled data set of focal mechanisms to estimate stress parameters and characterize the prevailing state of stress within ten of the main seismic zones of central and eastern North America. We compare our results with regional borehole stress information from the World Stress Map and Canadian Crustal Stress databases to determine the consistency of seismological and borehole estimates of the state of stress near the seismic zones and to elucidate potential stress perturbations associated with regionally elevated earthquake activity.

DATA SETS AND STRESS ESTIMATION TECHNIQUE

Focal Mechanisms

The earthquake focal mechanism data set is shown in Figure 1. (See supplementary material for references and focal mechanism octant plots.[1]) It constitutes mostly first-motion solutions complemented by a small number of moment tensors (~15% of the total). In most cases, a quality factor was provided in the original study in the form of a qualitative level (A–D) or a quantitative angular uncertainty. In order to obtain a coherent set of inversion results, we standardized these quality rankings by assigning small (±15°), medium (±25°), or large (±35°) uncertainties to each mechanism's strike, dip, and rake angles, which are assumed to be independent (cf. Walsh et al., 2009). In those cases in which the original study did not provide a quality level, we assigned an uncertainty level on the basis of the data-analysis description. In addition, focal mechanism uncertainties were adjusted on the basis of earthquake magnitudes to take into account the potentially higher uncertainty and lower quality of small-magnitude solutions: all $M < 2.5$ and $2.5 \le M < 3.5$ mechanisms were assigned large and medium uncertainties (±35° and ± 25°), respectively.

[1]GSA Data Repository Item 2010020, focal mechanism data set, octant plots, and Charlevoix stress analyses, is available at www.geosociety.org/pubs/ft2010.htm, or on request from editing@geosociety.org, Documents Secretary, GSA, P.O. Box 9140, Boulder, CO 80301-9140, USA.

We focus on ten of the main eastern North American seismic zones, which we define as areas encompassing more than five focal mechanisms within a distinct geological and seismological area (Fig. 1). The Lower St. Lawrence, Charlevoix, Montreal, and Eastern Tennessee zones are associated with the Iapetus rifted margin, and the Ottawa and New Madrid zones are associated with Iapetus failed rift arms (Adams and Basham, 1991; Wheeler, 1995). The Gatineau seismic zone may be related to the trace of the New England Seamount Chain hotspot (Adams and Basham, 1991). The North Appalachian, Central Virginia, and Charleston seismic zones are not affiliated with clear lithosphere-scale structures: in the first two, the seismicity occurs within the Appalachian formations that overlie rifted Grenville crust (Munsey and Bollinger, 1985; Adams and Basham, 1991). Other seismicity clusters can be identified in central and eastern North America, but the paucity of focal mechanisms precludes any stress analysis.

Seismological Stress Estimation

We used a Bayesian estimation technique (Arnold and Townend, 2007) to determine the set of stress parameters most consistent with the focal mechanisms in a given group. We weighted each focal mechanism by converting the aforementioned angular errors to a scalar Matrix Fisher concentration parameter (Equation A12 of Arnold and Townend, 2007). This approach yields a joint probability density function of the three angles specifying the principal stress axes' orientations and a single stress magnitude ratio parameter. Its principal advantages, in comparison with other stress estimation algorithms, are the incorporations of focal mechanism uncertainties, nodal plane ambiguity, and the weak constraint imposed on the stress tensor by any single focal mechanism. This last point is particularly important because it allows us to derive confidence intervals for the stress tensor parameters that take into account the degree of similarity between focal mechanisms within individual seismic zones (Arnold and Townend, 2007). As shown in the octant plots (supplementary material [see footnote 1]), the diversity of mechanisms can vary significantly between zones.

We computed the trend of the axis of maximum horizontal compressive stress (S_H) using the algorithm described by Lund and Townend (2007). Such a transformation is necessary when none of the three principal stresses is strictly vertical, and it enables all four determinable parameters to be amalgamated into a single, physically intuitive and readily illustrated parameter. This produces a probabilistic description of S_H from which we can compute the median trend and associated confidence intervals.

Borehole Stress Data

In order to perform a detailed comparison of our seismological stress estimates with borehole crustal stress measurements on a regional scale, we extracted stress magnitude and orientation data from the World Stress Map and the Canadian Crustal Stress databases (Zoback, 1992a; Adams, 1995; Heidbach et al., 2008). For each seismic zone, we calculated a weighted mean S_H orientation for borehole breakout and hydrofracture measurements with qualities of A, B, or C made at depths greater than 0.5 km within 250 km of each seismic zone. The weighted mean and its associated standard deviation were estimated by assigning weights of 3, 2, and 1 to the A, B, and C quality S_H measurements, respectively. In most cases, the borehole S_H data are located outside of the seismic zones and are unevenly distributed. Because of the strong regional coherence of the borehole stress orientations over distances of hundreds of kilometers (Zoback, 1992a), we assume that these 250 km S_H averages provide appropriate estimates of the regional stress orientation outside of the seismic zones.

RESULTS

Eastern North America

The results are shown in Figures 2 and 3 and listed in Table 1 in terms of median S_{HS} trend and 90% confidence interval ($90CI_S$); the subscript "S" is used to denote a seismological estimate. The 90% confidence interval is ~20°–40° in most cases. The Ottawa seismic zone stands out with a very large $90CI_S$ of 132°, indicating that the directions of the principal horizontal stresses are not constrained by this small data set (eight mechanisms, two of which have large uncertainties). The results for this zone are not used for further discussion.

In all but one case, the estimated S_{HS} orientation lies in the NE-SW quadrant, roughly parallel to the general S_{HB} trend inferred from borehole measurements (Fig. 3); the subscript "B" is used to denote a borehole estimate. For the New Madrid, Eastern Tennessee, Montreal, and Gatineau seismic zones, the median seismological and average borehole S_H orientations (S_{HS} and S_{HB}, respectively) are consistent to within 5°–15°, well within the respective 90% confidence intervals. The lack of borehole S_{HB} data within 250 km of the Charleston seismic zone precludes a direct comparison with the S_{HS} orientation. However, the nearest S_{HB} measurement (C quality at

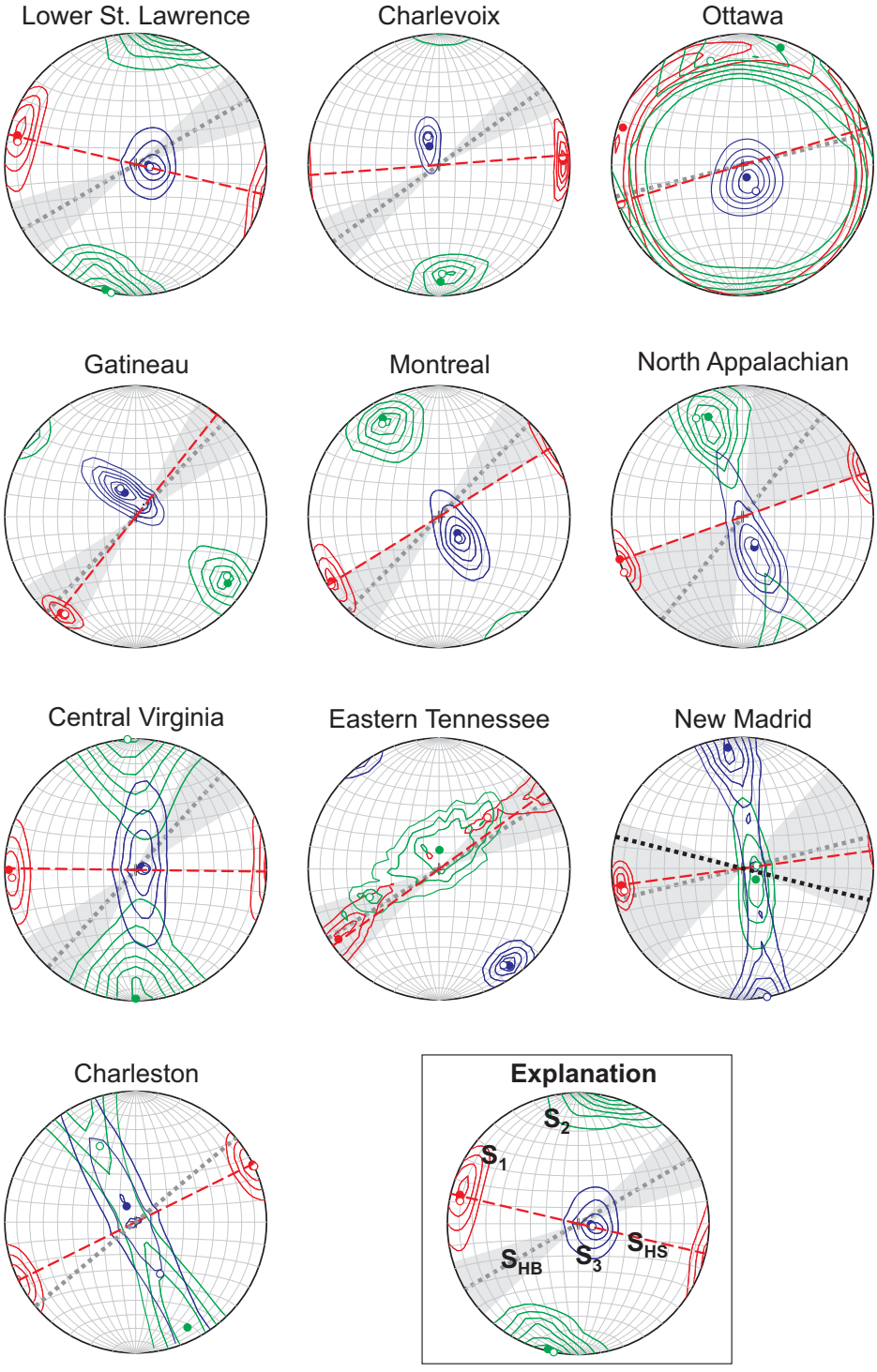

Figure 2. State of stress in seismic zones. Lower-hemisphere stereonets show the posterior distributions of the principal stress axes (S_1—red, S_2—green, S_3—blue). Dashed red lines indicate the median orientation of the seismologically determined maximum horizontal compressive stress S_{HS}. Dotted gray lines and gray angular sectors indicate the average and 90% confidence region of the maximum horizontal compressive stress from borehole data S_{HB} (Table 1). New Madrid: The black dotted line shows the S_1 orientation for the Bardwell earthquake sequence (Horton et al., 2005).

255 km) has an orientation that lies within the 90% confidence interval of S_{HS} (Fig. 2). For the North Appalachian seismic zone, the median S_{HS} and average S_{HB} values differ by 33°, but the 90% confidence intervals overlap by 13° (Fig. 2). The three remaining seismic zones (Central Virginia, Lower St. Lawrence, and Charlevoix) show statistically significant differences between S_{HS} and S_{HB} azimuths and are discussed in more detail in the following sections.

Central Virginia Seismic Zone

The state of stress in the Central Virginia seismic zone was determined by the focal mechanisms of 11 small earthquakes (M < 3) recorded during 4 yr in the early 1980s (Munsey and Bollinger, 1985), complemented by two M ~4 earthquakes that occurred in 2003. These events all occurred at regionally typical depths shallower than ~15 km within the allochthonous, thrust-faulted, Appalachian formations that override the Precambrian Grenville basement (Bollinger et al., 1985; Munsey and Bollinger, 1985).

The S_{HS} orientation is rotated 48° clockwise with respect to the regional borehole S_{HB} trend, and the 90% confidence intervals of S_{HS} and S_{HB} are separated by 13° (Table 1; Fig. 2), indicating that the two estimates are significantly distinct. Using the same data set, excluding the 2003 events, Kim and Chapman (2005) inferred a slightly larger clockwise rotation of S_{HS} relative to S_{HB} (~68°), with an azimuth and plunge of N133° and 14°SE for the S_1 axis (cf. N086° and 7°W for our results; Fig. 2). The difference in orientation and plunge of S_1 between the two analyses may be in part due to the difference in the stress inversion technique (Bayesian versus grid-search). Alternatively, the difference in results may reflect the small difference in the data sets in relation to the complexity of the seismological state of stress in the Central Virginia seismic zone. The 13 focal mechanisms have P axis orientations in both NE-SW and NW-SE directions, suggesting that the stress regime may change from mainly thrust to mainly strike slip with depth (Munsey and Bollinger, 1985).

Lower St. Lawrence Seismic Zone

The Lower St. Lawrence seismic zone is delineated by pronounced microseismicity located mainly beneath the St. Lawrence River (Fig. 1) (Adams and Basham, 1991). The best-constrained hypocenters place the earthquakes between 7 and 25 km depth, within the rifted Precambrian Grenville basement and well below the overthrust Appalachian formations (Adams and Basham, 1991; Lamontagne et al., 2003).

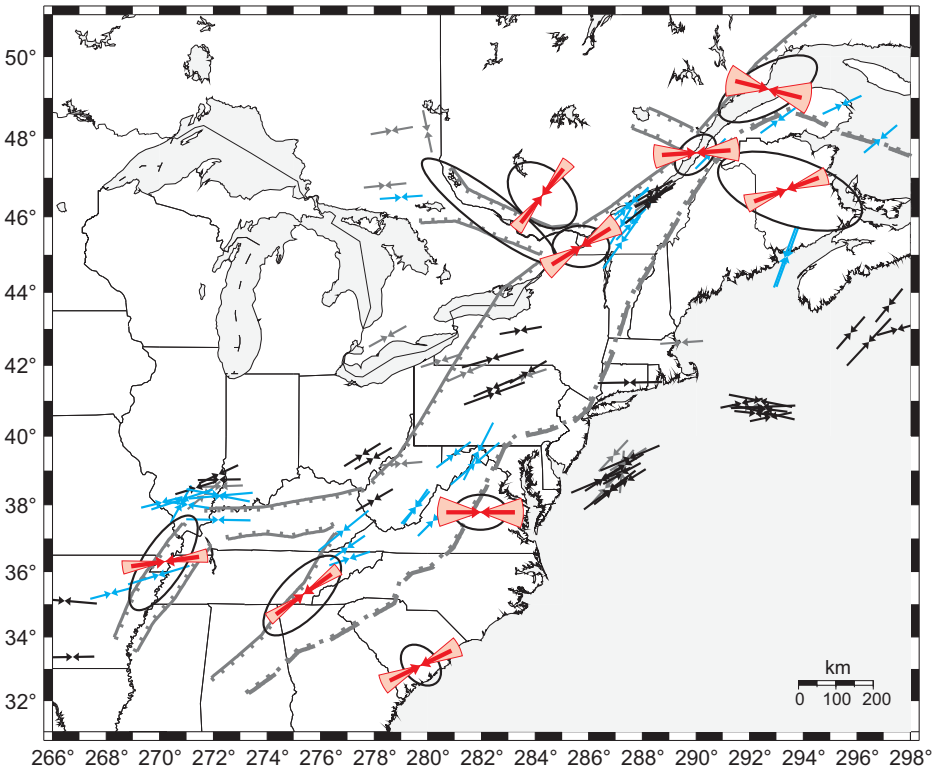

Figure 3. Eastern North America maximum horizontal compressive stress. Solid and gray arrows indicate S_{HB} orientation from borehole observations (A and B–C quality, respectively). Blue arrows indicate borehole observations used in calculating the regional average within 250 km of the seismic zones (solid ellipses). Red arrows and angular sectors indicate S_{HS} orientation from focal mechanism inversion (median and 90% range, Table 1).

TABLE 1. STRESS INVERSION RESULTS VERSUS LOCAL BOREHOLE STRESS ORIENTATION

Seismic zone	Seismological stress				Borehole stress		
	N_S	S_{HS} (°)	$90CI_S$ (°)	R	N_B	S_{HB} (°)	$90CI_B$ (°)
Lower St. Lawrence	12	104 (R)	081–124	0.4	2	060	46–73
Charlevoix	60	086 (R)	069–101	0.3	12	054	43–65
Charlevoix NW	25	055 (R)	035–074	0.2	12	054	43–65
Charlevoix SE	35	101 (R)	086–114	0.4	12	054	43–65
Gatineau	19	038 (R)	029–048	0.8	6	043	28–58
Ottawa	8	078 (R)	001–133	0.3	1	086	—
Montreal	21	058 (R)	043–073	0.4	7	044	30–59
North Appalachian	12	070 (R)	059–083	0.6	5	038	5–71
Central Virginia	13	090 (R)	071–111	0.7	6	042	26–58
East Tennessee	26	054 (S)	046–063	0.2	3	058	43–73
New Madrid	18	082 (S)	073–091	0.9	10	076	41–111
Charleston	11	064 (S)	050–077	1.0	1	040*	—

Note: N_S—number of focal mechanisms; S_{HS} and $90CI_S$—median and 90% confidence interval azimuth of the axis of maximum horizontal compressive stress (R—reverse, S—strike-slip); R—median stress ratio $(S_1 - S_2)/(S_1 - S_3)$; N_B—number of borehole data; S_{HB} and $90CI_B$—weighted average and 90% confidence interval azimuth of the borehole axis of maximum horizontal compression within 250 km of the seismic zone.
*Based on nearest borehole at 255 km.

Although tentative correlations have been made between the earthquakes and the Iapetus Rift faults, most of the seismicity appears to occur within fractured volumes of the rift system rather than on the main rift faults themselves (Lamontagne et al., 2003).

The S_{HS} orientation is rotated 44° clockwise compared to the regional borehole stress orientation S_{HB} (Table 1; Fig. 2). The 90% confidence intervals for the two estimates are separated by 8°, indicating a statistically significant difference. There are two important caveats with regard to this observation: (1) the S_{HB} orientation and standard error are only based on two B quality data points (individual azimuths of 54° and 65°; Fig. 3); and (2) the S_{HS} orientation is only defined by 12 mechanisms, exhibiting a relatively low diversity and hence yielding a relatively large $90CI_S$ value. Notwithstanding these points, the seismological versus borehole stress rotation appears to be robust, and the borehole S_{HB} orientation is similar to the general direction for eastern Canada (Fig. 3). The seismological S_{HS} value is stable for several tested combinations of eight or more (out of 12) mechanisms and yields a S_{HS} orientation between N100° and N120°, in all cases strongly oblique to the regional borehole data.

Charlevoix Seismic Zone

The Charlevoix seismic zone is one of the historically most active earthquake concentrations in eastern North America, with five $M \geq 6$ earthquakes since 1663 (Lamontagne, 1987; Adams and Basham, 1991). Most earthquakes occur between 5 and 25 km depth beneath the St. Lawrence River. The main geological structures are related to the ca. 1100 Ma Grenville orogeny, ca. 650 Ma Iapetus rifting, ca. 450 Ma Appalachian orogeny, and a large meteor impact ca. 350 Ma. Using remote-sensing, seismic, and potential field data, Lamontagne et al. (2000) identified the Saint-Laurent and Charlevoix faults (Fig. 4) as the main Iapetus Rift faults and the principal structures in the seismic zone.

No clear association can be found between the seismicity and the main fault structures (e.g., Lamontagne et al., 2000), but a first-order NW-SE clustering pattern is apparent in the earthquakes' epicenters. As shown in Figure 4, a largely aseismic, ~5-km-wide zone separates two distinct microseismicity clusters to the southeast (mostly beneath the river) and the northwest (mostly beneath the north shore; Anglin and Buchbinder, 1981). This gap coincides with an elongated high-seismic-velocity body (Vlahovic et al., 2003) and with the location of the Saint-Laurent fault (Fig. 4, cross section).

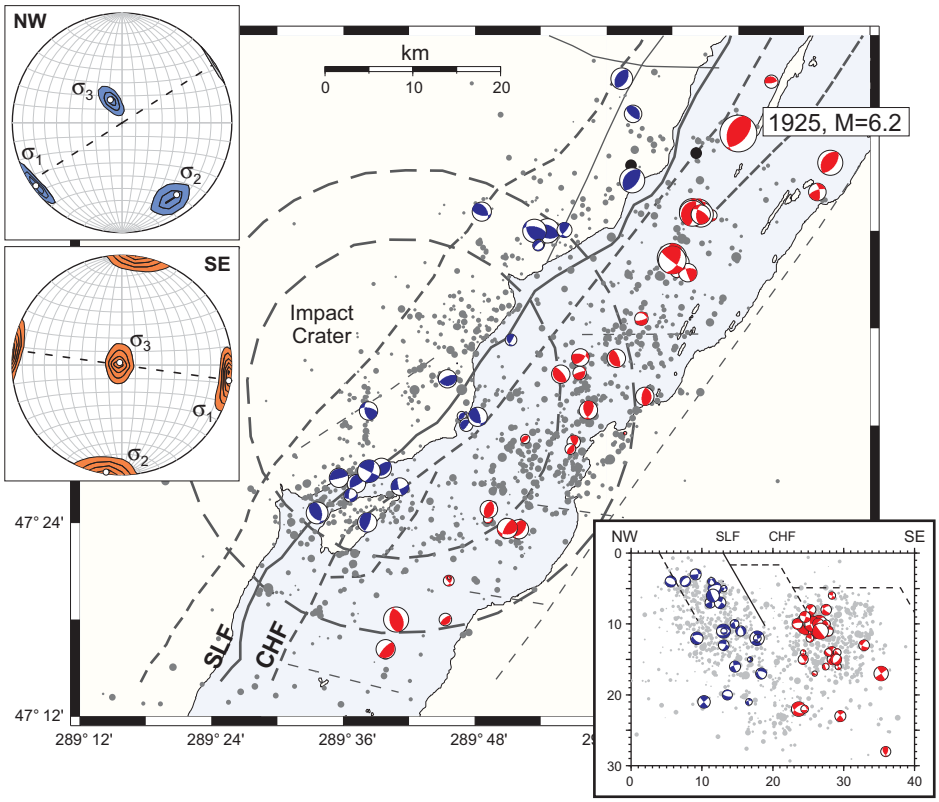

Figure 4. Charlevoix maximum horizontal compressive stress. Earthquakes and focal mechanisms are as in Figure 1. Solid and dashed lines show Iapetus Rift faults and impact crater structure (Lamontagne et al., 2000). SLF—Saint-Laurent fault; CHF—Charlevoix fault. Lower-right insert shows a NW-SE depth cross section. The upper-left insert shows stereonets of the state of stress from inversion of focal mechanisms to the northwest (blue) and southeast (red) of the Saint-Laurent fault.

Analysis of the 60 focal mechanisms in the Charlevoix seismic zone yields a S_{HS} orientation of N086°, rotated 32° clockwise relative to the regional S_{HB} from nearby boreholes (Table 1; Fig. 2). The 90% confidence intervals for the two estimates are distinct by 4°. The large number of focal mechanisms allows us to test for spatial variations in stress orientations amongst subsets of events. The most significant difference in S_{HS} orientation exists between the focal mechanism clusters to the southeast and northwest of the Saint-Laurent fault (Fig. 4). For the northwest group, S_{HS} is oriented N055°, parallel to the regional borehole data, whereas S_{HS} for the southeast group is oriented N101° and rotated clockwise by 47° compared to the borehole trend (Table 1; Fig. 4). This rotation is significant at the 90% confidence level, with a separation of 21° between the seismological and borehole confidence intervals. Various earthquake grouping and inversion tests (supplementary material [see footnote 1]) indicate that the NW-SE clustering is the grouping associated with the most significant rotation.

The 1925 Charlevoix M = 6.2 earthquake ruptured a steeply dipping thrust fault striking parallel to the regional S_H orientation (Bent, 1992; Fig. 4). The rotated S_{HS} observed for the southeast side of the Charlevoix seismic zone is more compatible than the regional S_H direction with the focal mechanism of the 1925 event, as well as with numerous smaller thrust events that have fault planes striking NE-SW.

DISCUSSION

Consistency and Extent of Stress Rotations

Out of the ten seismic zones addressed in this study, the Central Virginia, Lower St. Lawrence, and Charlevoix seismic zones each show a 30°–50° clockwise rotation of the seismic S_{HS} orientation relative to the regional borehole S_{HB} orientation that is significant at the 90% confidence level. A similar clockwise rotation of 32° is observed for the North Appalachian seismic zone, albeit with a 12° overlap of the seismological and borehole 90% confidence intervals (Fig. 2). Although not statistically significant, that result is worth noting in comparison with the 48° clockwise rotation observed in the Central Virginia seismic zone: both seismic zones exhibit clusters of earthquakes confined to the shallow (<15 km) Appalachian formations that override the deeper Grenville basement (Bollinger et al., 1985; Adams and Basham, 1991).

A similar, although slightly smaller, clockwise rotation can be deduced for the 2003 M = 4.0 Bardwell earthquake sequence north of the New Madrid seismic zone. For the main shock and aftershock sequence, Horton et al. (2005) derived a S_1 orientation of N104° with an uncertainty of approximately ±20°. Assuming that $S_{HS} = S_1$, this result indicates a clockwise rotation of 20°–30° compared to our median estimates of S_{HS} for the New Madrid focal mechanisms (excluding the Bardwell sequence) and S_{HB} from nearby borehole data (Table 1; Fig. 2). Although not statistically significant, this apparent rotation suggests that large variations in stress orientation can occur over a distance of ~40 km in the New Madrid–Wabash Valley area (Horton et al., 2005), similar to the ~20 km distance that separates the two seismic clusters in the Charlevoix seismic zone.

It is important to consider whether the apparent stress rotations are artifacts stemming from the comparison between relatively shallow borehole data (0.5–2 km) and deeper seismicity (1–30 km). Vertical variations in stress orientations have been reported over depth intervals of 100–1000 m in individual boreholes (e.g., Hickman and Zoback, 2004), but in general, deep borehole- and earthquake-determined stress orientations are similar and can be jointly accounted for in terms of, for instance, dynamical modeling results (e.g., Townend and Zoback, 2004). Moreover, the eastern and western Charlevoix results are based on earthquakes at comparable depths. Hence, we consider it unlikely that the observed rotations are depth-related artifacts.

Overall, therefore, we find that the angular difference between S_{HS} and S_{HB} exhibits a bimodal pattern: four seismic zones exhibit good agreement between seismological and borehole estimates of the S_H orientation (Gatineau, Montreal, Eastern Tennessee, and New Madrid), and five imply 30°–50° clockwise rotations of the seismological S_{HS} relative to the regional borehole S_{HB} (Lower St. Lawrence, Charlevoix, Central Virginia, and, to a lesser extent, North Appalachian and Bardwell–northern New Madrid). In the case of the Lower St. Lawrence, Central Virginia, and North Appalachian, the rotation between S_{HS} inside the seismic zone and S_{HB} outside the seismic zone occurs over distances of 50–100 km (Fig. 3). For Charlevoix and Bardwell–northern New Madrid, the rotation occurs over 20–40 km (Fig. 4). In the following section, we consider the magnitude and potential causes of the stress perturbation required to

account for the 30°–50° clockwise rotation of the horizontal principal stresses over such short distances.

Magnitude of the Stress Perturbations

In order to obtain a first-order estimate of the stress perturbation causing the observed rotations, we consider the model of Sonder (1990) and Zoback (1992a). In this model, the orientation of the maximum horizontal compressive stress (represented here by S_{HS}) in the vicinity of a major structure can be calculated in terms of a regional stress orientation (represented here by S_{HB}) and a uniaxial stress perturbation (S_L) orthogonal to the strike of the structure. We assume that, for the Charlevoix, Lower St. Lawrence, and Central Virginia seismic zones, the stress responsible for the local rotation is perpendicular to the average local Iapetus Rift direction (Fig. 1). With this assumption, the magnitude of the uniaxial stress perturbation S_L is found using Equation 8 of Zoback (1992a) to be 80%–110% that of the regional horizontal differential stress (i.e., $[S_H - S_h]/S_L \sim 0.8–1.1$; Table 2).

Deep intraplate borehole data from a number of locations worldwide reveal that at depths of as much as 8 km, the crust is in a state of stress consistent with incipient frictional failure given coefficients of friction $\mu \approx 0.6–1.0$ and the observed near-hydrostatic pore-fluid pressures ($\lambda \approx 0.4$; Townend and Zoback, 2000). Similarly, stress magnitude data from boreholes in central and eastern North America (Adams and Bell, 1991; Adams, 1995; Heidbach et al., 2008) show a relationship between differential stress ($S_1 - S_3$) and effective mean stress that is consistent with incipient frictional failure for coefficients of friction $\mu > 0.5$ (Fig. 5). Also illustrated in Figure 5, a histogram of stress ratio measurements from the same boreholes exhibits a pronounced peak at $0.5 \le R_B \le 0.8$ and mean of $R_B = 0.6$, with few values smaller than 0.4. The majority of these borehole stress measurements are located in the Canadian Shield, west and north of the main seismic zones. Thus, they may be considered as constituting a reference state of stress for the continental crust outside of seismically active regions.

If we assume that the stress magnitude parameters in each seismic zone are similar to those in intraplate continental crust as a whole ($\mu = 0.8$, $\lambda = 0.4$, $R = 0.6$, $\rho = 2700$ kg m^{-3}; see Appendix A for details), the differential stress in the horizontal plane at a mid-seismogenic zone depth of 8 km is $S_H - S_h = S_1 - S_2 \approx 250$ MPa for a reverse stress state, and $S_H - S_h = S_1 - S_3 \approx 160$ MPa for a strike-slip stress state. This analysis suggests that a local stress perturbation S_L of comparable magnitude is required to locally reorient S_{HB} by 30°–50°, as implied by the Lower St. Lawrence, Charlevoix, and Central Virginia stress orientation results.

Such high stress magnitudes clearly depend on the assumed friction coefficient and the fluid pressure regime. If we assume that either a low friction coefficient ($\mu = 0.1$) or a near-lithostatic pore-fluid pressure ($\lambda \approx 0.9$) prevails in the seismic zones, the horizontal differential stress and the corresponding stress perturbation S_L would be of the order of only ~20–40 MPa. However, the low ambient stress magnitudes implied by those parameters contrast markedly with the values thought to characterize aseismic or low-seismicity intraplate continental crust as a whole, as outlined herein (Fig. 5).

Potential Sources of the Stress Perturbations

The consistency of the 30°–50° clockwise stress rotations observed from the St. Lawrence valley to the central Appalachians (and possibly to the New Madrid–Wabash Valley) suggests a similar mechanism or source for seismic zones separated by large distances. The calculations discussed in the previous section imply a stress perturbation at mid-seismogenic depths of 160–250 MPa (in a representative high-friction, low-fluid-pressure case) or 20–40 MPa (low friction or high fluid pressure) and a maximum horizontal stress S_L trending approximately N115°–135° (Table 2).

Various mechanisms have been proposed as potential sources of local and regional stress perturbations, including topography, crustal density anomalies, fault intersections, flexure under local loads (e.g., sedimentary basins), and postglacial rebound (e.g., Stein et al., 1989; Talwani, 1988; Zoback, 1992a; Assameur and Mareschal, 1995). Most of these mechanisms account for stress perturbations of at most a few tens of megapascals and would only result in significant horizontal stress rotations if prevailing horizontal stresses were at the low end of stress levels calculated here. Flexural stresses may reach several hundred megapascals under sediment loads of 10 km thickness (Stein et al., 1989), but such conditions do not appear

TABLE 2. STRESS PERTURBATION MAGNITUDE AND ORIENTATION

Seismic zone	Structure (°)	S_{HB} (°)	S_{HS} (°)	θ (°)	γ (°)	$(S_H - S_h)/S_L$	S_L (°)
Lower St. Lawrence	045	060	104	15	44	0.88	135
Charlevoix	035	054	086	19	32	1.09	125
Central Virginia	027	042	090	15	48	0.81	117

Note: Structure—average azimuth of primary regional structural direction; S_{HS} and S_{HB}—azimuth of axis of maximum horizontal compressive stress from seismic inversion and borehole data (cf. Table 1). $\theta = S_{HB} -$ structure; $\gamma = S_{HS} - S_{HB}$. $(S_H - S_h)/S_L$ is ratio of local horizontal differential stress to stress perturbation (S_L, cf. text and Sonder, 1990). S_L—azimuth of stress perturbation.

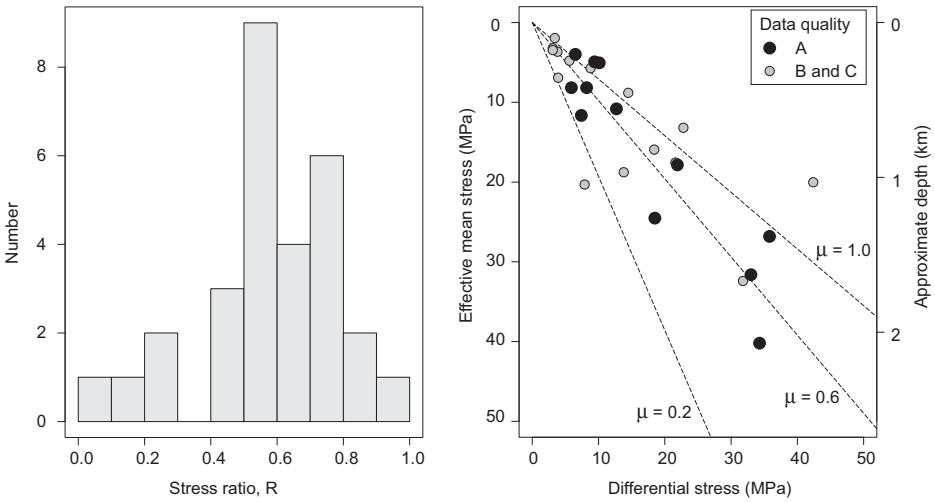

Figure 5. Stress ratio and differential stress from borehole data. Left: Histogram of stress ratio R = $(S_1 - S_3)/(S_2 - S_3)$ from A, B, and C quality borehole stress measurements deeper than 0.5 km in eastern North America. Right: Differential stress ($S_1 - S_3$) versus effective mean stress (mean stress minus pore fluid pressure) from borehole stress measurements deeper than 0.1 km of quality A (open circles) and B or C (solid circles) in eastern North America.

applicable to continental seismic zones. Similarly, large crustal density anomalies have been demonstrated to produce stress perturbations of as much as ~200 MPa and rotations of up to 90° (Zoback and Richardson, 1996). However, gravity and seismic velocity data do not indicate the presence of widespread high-density anomalies associated with the Iapetus Rift structures in the Charlevoix and Lower St. Lawrence seismic zones (Lamontagne et al., 2000, 2003).

One possible mechanism by which consistent local stress perturbations may be generated over large distances is the concentration of postglacial rebound stresses by local zones of weakness, perhaps including low-friction faults. Postglacial rebound stresses show a strong spatial coherence over distances of thousands of kilometers, but they are typically smaller than ~10 MPa (e.g., Wu and Hasegawa, 1996). However, the presence of a "weak zone" in the lithosphere, such as low upper-mantle viscosity or a low-friction fault in the crust, can result in stress amplifications by a factor of 5–10 with respect to homogeneous lithosphere models (e.g., Grollimund and Zoback, 2001; Wu and Mazzotti, 2007). In such cases, the modulation of large-scale, small-amplitude postglacial rebound stresses by local zones of weakness could produce perturbations that are coherent over large distances but only affect those areas with locally reduced horizontal differential stress levels. In other words, postglacial rebound stresses may be high enough to reorient the local stress field surrounding faults with low friction or other properties that maintain ambient stress at levels lower than in the "typical low-seismicity" continental intraplate crust.

The St. Lawrence Valley may provide possible examples of this mechanism. In both the Lower St. Lawrence and Charlevoix seismic zones, the estimated S_{HS} orientation is strongly oblique to the regional S_{HB} orientation derived from borehole data located 30–100 km outside the seismic zones (Fig. 3). In Charlevoix, the relationships between the seismicity distribution and geological structures jointly suggest that the main rift faults may have unusually low friction ($\mu \sim 0.1$; Baird et al., 2009). Recent models of postglacial rebound stress and strain that incorporate a weak zone in the lithosphere beneath the St. Lawrence Valley show a significant amplification and clockwise rotation of the postglacial rebound stresses directly above the weak zone (Wu and Mazzotti, 2007). The resulting postglacial rebound horizontal stress and strain orientations are nearly parallel to our estimated S_{HS} orientation and to the maximum horizontal contraction rate measured by global positioning system in the Charlevoix and Lower St. Lawrence seismic zones (Mazzotti et al., 2005, 2006).

CONCLUSIONS

(1) Comparisons of the axis of maximum horizontal compressive stress determined from earthquake focal mechanisms in seismic zones (S_{HS}) and from borehole data near but outside the seismic zones (S_{HB}) reveal a bimodal pattern: S_{HS} and S_{HB} are closely parallel in four seismic zones (Gatineau, Montreal, Eastern Tennessee, and New Madrid); in three other zones (Lower St. Lawrence, Charlevoix, and Central Virginia), S_{HS} is rotated 30°–50° clockwise compared to S_{HB}; two other zones (North Appalachian and Bardwell–northern New Madrid) show indications of similar clockwise rotations but at a low confidence level.

(2) The observed S_{HS} versus S_{HB} rotations are similar in both sense and magnitude in seismic zones separated by up to ~1500 km.

(3) The observed S_{HS} versus S_{HB} rotations occur over distances of no more than 50–100 km. In two cases (SE versus NW Charlevoix and Bardwell versus New Madrid), the rotation appears to occur over a distance of 20–50 km.

(4) With respect to a simple model of stress rotations near structural boundaries, the observed S_{HS} versus S_{HB} rotations imply a local stress perturbation of 160–250 MPa at a representative depth of 8 km. This assumes that the crust in the seismic zones is in a state of stress similar to that of "typical, low-seismicity" continental crust as a whole, namely, incipient frictional failure with coefficients of friction $\mu \approx 0.6$–1.0 and near-hydrostatic pore-fluid pressures. If the seismic zones were characterized by either a very low coefficient of friction ($\mu = 0.1$) or a near-lithostatic pore-fluid pressure, the required stress perturbation according to the model used here would be only 20–40 MPa.

(5) Local stress perturbations associated with fault intersections or large density anomalies could be sufficiently large (hundreds of megapascals) to account for the observed rotations, but their short wavelength (~10–100 km) cannot explain similar S_{HS} rotations over 1500 km (point 2).

(6) Long-wavelength (hundreds of kilometers) stress perturbation mechanisms such as topography, basin flexure, and postglacial rebound are typically associated with stress magnitudes of the order of tens of megapascals and thus cannot straightforwardly account for the observed S_{HS} rotations if midcrustal stress magnitudes are of the order of hundreds of megapascals (point 4).

(7) A possible mechanism for similar stress perturbations over large distances is the concentration of postglacial rebound stresses by local zones of weakness, such as low-friction faults. This would result in long-wavelength perturbations affecting only the weak zones. The Lower St. Lawrence and Charlevoix seismic zones may be examples of such mechanism, where the S_{HS} orientation in the seismic zones is parallel to that predicted by postglacial rebound models that incorporate a local weak zone (Mazzotti et al., 2006).

APPENDIX A. STRESS MAGNITUDES

To estimate the regional stress magnitudes, we adopt the critically stressed crust model of Townend and Zoback (2000) in which the state of stress in the crust is controlled by optimally oriented Andersonian faults on the brink of frictional failure equilibrium. In this case, the maximum and minimum effective stresses, $S_1 - P_f$ and $S_3 - P_f$, are related by:

$$\frac{S_1 - P_f}{S_3 - P_f} = \left(\sqrt{\mu^2 + 1} + \mu\right)^2 \equiv F, \qquad \text{(A1)}$$

where P_f is the pore-fluid pressure, and μ the coefficient of friction (see Zoback and Townend, 2001, and references therein).

In normal, strike-slip, and reverse stress states, the effective vertical stress S_V is:

$$S_v = (1-\lambda)\,pgz = \begin{cases} S_1 & \text{normal} \\ S_2 & \text{strike-slip} \\ S_3 & \text{reverse} \end{cases}, \qquad \text{(A2)}$$

where ρ is the average crustal density, g is the gravitational acceleration, z is the depth, and $\lambda = P_f/S_v$ is the pore-fluid factor. In each case, we can express all three principal stresses in terms of the vertical stress S_V and the differential stress $\Delta S = S_1 - S_3$, and solve Equation A1 to obtain ΔS as a function of depth and the frictional parameter F. This yields:

$$\Delta S = pgz(\lambda - 1)(1 - F) \times \begin{cases} 1/F & \text{normal} \\ 1/\left(R + (1-R)F\right) & \text{strike-slip} \\ 1 & \text{reverse} \end{cases}, \qquad \text{(A3)}$$

where the stress ratio

$$R = \frac{S_1 - S_2}{S_1 - S_3} = \frac{S_1 - S_2}{\Delta S} \qquad \text{(A4)}$$

appearing in the strike-slip case is used to explicitly relate the intermediate principal stress to the differential stress. Expressions A2–A4 can be used to compute all three principal stress magnitudes and hence, given the orientation of the maximum horizontal stress, fully determine the stress tensor.

ACKNOWLEDGMENTS

We thank John Adams and Mark Zoback for ongoing discussions about eastern North America stress and seismicity, John Cassidy and Roy Hyndman for comments on a preliminary version of the manuscript, and Björn Lund for very detailed input during the review process. Allison

Bent, Shutien Ma, Pradeed Talwani, and Maurice Lamontagne provided focal mechanisms and data assistance, and Ikuko Wada helped with an early analysis. This is Geological Survey of Canada contribution 20080471.

REFERENCES CITED

Adams, J., 1995, The Canadian Crustal Stress Database—A compilation to 1994: Geological Survey of Canada Open-File 3122, 437 p.

Adams, J., and Basham, P.W., 1991, The seismicity and seismotectonics of eastern Canada, *in* Slemmon, B., et al., eds., The Geology of North America, Decade Map Volume 1, Neotectonics of North America: Boulder, Colorado, Geological Society of America, p. 261–276.

Adams, J., and Bell, J.S., 1991, Crustal stress in Canada, *in* Slemmon, B., et al., eds., The Geology of North America, Decade Map Volume 1, Neotectonics of North America: Boulder, Colorado, Geological Society of America, p. 367–386.

Anglin, F., and Buchbinder, G., 1981, Microseismicity in the mid–St. Lawrence Valley Charlevoix zone, Quebec: Bulletin of the Seismological Society of America, v. 71, p. 1553–1560.

Arnold, R., and Townend, J., 2007, A Bayesian approach to estimating tectonic stress from seismological data: Geophysical Journal International, v. 170, p. 1336–1356, doi: 10.1111/j.1365-246X.2007.03485.x.

Assameur, D.M., and Mareschal, J.C., 1995, Stress induced by topography and crustal density heterogeneities: Implication for the seismicity of southeastern Canada: Tectonophysics, v. 241, p. 179–192, doi: 10.1016/0040-1951(94)00202-K.

Baird, A.F., McKinnon, S.D., and Godin, L., 2009, Stress channeling and partitioning of seismicity in the Charlevoix seismic zone, Quebec, Canada: Geophysical Journal International, v. 179, p. 559–568, doi: 10.1111/j.1365-246X.2009.04275.x.

Bent, A.L., 1992, A re-examination of the 1925 Charlevoix, Quebec, earthquake: Bulletin of the Seismological Society of America, v. 82, p. 2097–2113.

Bollinger, G.A., Chapman, M.C., Sibol, M.S., and Costain, J.K., 1985, Analysis of earthquake focal depths in the southeastern U.S.: Geophysical Research Letters, v. 12, p. 785–788, doi: 10.1029/GL012i011p00785.

Grollimund, B., and Zoback, M.D., 2001, Did deglaciation trigger New Madrid seismicity?: Geology, v. 29, p. 175–178, doi: 10.1130/0091-7613(2001)029<0175:DDTISI>2.0.CO;2.

Heidbach, O., Tingay, M., Barth, A., Reinecker, J., Kurfeß, D., and Müller, B., 2008, The Release 2008 of the World Stress Map: http://www.world-stress-map.org (June 2009).

Hickman, S., and Zoback, M.D., 2004, Stress orientations and magnitudes in the SAFOD pilot hole: Geophysical Research Letters, v. 31, L15S12, doi: 10.1029/2004GL020043.

Horton, S.P., Kim, W.Y., and Withers, M., 2005, The 6 June 2003 Bardwell, Kentucky, earthquake sequence: Evidence for a locally perturbed stress field in the Mississippi embayment: Bulletin of the Seismological Society of America, v. 95, p. 431–445, doi: 10.1785/0120040052.

Johnston, A.C., Coppersmith, K.J., Kanter, L.R., and Cornell, C.A., 1994, The earthquakes of stable continental regions: Assessment of large earthquake potential, *in* Schneider, J.F., ed., Electronic Power Research Institute Report TR-102261: Palo Alto, California, Electronic Power Research Institute, 309 p.

Kim, W.-Y., and Chapman, M., 2005, The 9 December 2003 Central Virginia earthquake sequence: A compound earthquake in the Central Virginia seismic zone: Bulletin of the Seismological Society of America, v. 95, p. 2428–2445, doi: 10.1785/0120040207.

Lamontagne, M., 1987, Seismic activity and structural features in the Charlevoix region, Quebec: Canadian Journal of Earth Sciences, v. 24, p. 2118–2129, doi: 10.1139/e87-202.

Lamontagne, M., Keating, P., and Toutin, T., 2000, Complex faulting confounds earthquake research in the Charlevoix seismic zone, Québec: Eos (Transactions, American Geophysical Union), v. 81, no. 26, p. 289, doi: 10.1029/00EO00213.

Lamontagne, M., Keating, P., and Perreault, S., 2003, Seismotectonic characteristics of the Lower St. Lawrence seismic zone, Quebec: Insights from geology, magnetics, gravity, and seismics: Canadian Journal of Earth Sciences, v. 40, p. 317–336, doi: 10.1139/e02-104.

Lund, B., and Townend, J., 2007, Calculating horizontal stress orientations with full or partial knowledge of the tectonic stress tensor: Geophysical Journal International, v. 170, p. 1328–1335, doi: 10.1111/j.1365-246X.2007.03468.x.

Mazzotti, S., James, T.S., Henton, J., and Adams, J., 2005, GPS crustal strain, postglacial rebound, and seismicity in eastern North America: The Saint Lawrence Valley example: Journal of Geophysical Research, v. 110, B11301, doi: 10.1029/2004JB003590.

Mazzotti, S., Wu, P., Wada, I., Adams, J., and Bent, A., 2006, Role of plate tectonic and postglacial rebound forces in the present-day state of stress and fault reactivation along the St. Lawrence and Ottawa Valleys: Geological Association of Canada Meeting Abstracts, v. 31, p. 99.

Munsey, J.W., and Bollinger, G.A., 1985, Focal mechanism analyses for Virginia earthquakes: Bulletin of the Seismological Society of America, v. 75, p. 1613–1636.

Richardson, R.M., 1992, Ridge forces, absolute plate motion, and the intraplate stress field: Journal of Geophysical Research, v. 97, no. B8, p. 11,739–11,748, doi: 10.1029/91JB00475.

Sonder, L.J., 1990, Effects of density contrasts on the orientation of stresses in the lithosphere: Relation to principal stress directions in the Transverse Ranges, California: Tectonics, v. 9, p. 761–771, doi: 10.1029/TC009i004p00761.

Stein, S., and Mazzotti, S., eds., 2007, Continental Intraplate Earthquakes: Science, Hazard, and Policy Issues: Boulder, Colorado, Geological Society of America Special Paper 425, 402 p.

Stein, S., Cloetingh, S., Sleep, N.H., and Wortel, R., 1989, Passive margin earthquakes, stresses and rheology, *in* Gregersen, S., and Basham, P., eds., Earthquakes at North-Atlantic Passive Margins: Neotectonics and Postglacial Rebound: NATO ASI Series C: Boston Massachusetts, Kluwer, p. 231–259.

Talwani, P., 1988, The intersection model for intraplate earthquakes: Seismological Research Letters, v. 59, p. 305–310.

Townend, J., and Zoback, M.D., 2000, How faulting keeps the crust strong: Geology, v. 28, p. 399–402, doi: 10.1130/0091-7613(2000)28<399:HFKTCS>2.0.CO;2.

Townend, J., and Zoback, M.D., 2004, Regional tectonic stress near the San Andreas fault in central and southern California: Geophysical Research Letters, v. 31, L15S11, doi: 10.1029/2003GL018918.

Vlahovic, G., Powell, C., and Lamontagne, M., 2003, A three-dimensional P wave velocity model for the Charlevoix seismic zone, Quebec, Canada: Journal of Geophysical Research, v. 108, no. B9, p. 2439, doi: 10.1029/2002JB002188.

Walsh, D., Arnold, R., and Townend, J., 2009, A Bayesian approach to determining and parameterizing earthquake focal mechanisms: Geophysical Journal International, v. 176, p. 235–255, doi: 10.1111/j.1365-246X.2008.03979.x.

Wheeler, R.L., 1995, Earthquakes and the cratonward limit of lapetan faulting in eastern North America: Geology, v. 23, p. 105–108, doi: 10.1130/0091-7613(1995)023<0105:EATCLO>2.3.CO;2.

Wu, P., and Hasegawa, H., 1996, Induced stresses and fault potential in eastern Canada due to a realistic load: A preliminary analysis: Geophysical Journal International, v. 127, p. 215–229, doi: 10.1111/j.1365-246X.1996.tb01546.x.

Wu, P., and Mazzotti, S., 2007, Effects of a lithospheric weak zone on postglacial seismotectonics in eastern Canada and northeastern USA, *in* Stein, S., and Mazzotti, S., eds., Continental Intraplate Earthquakes: Science, Hazard, and Policy Issues: Geological Society of America Special Paper 425, p. 113–128, doi:10.1130/2007.9425(09).

Zoback, M.D., and Townend, J., 2001, Implications of hydrostatic pore pressures and high crustal strength for the deformation of intraplate lithosphere: Tectonophysics, v. 336, p. 19–30, doi: 10.1016/S0040-1951(01)00091-9.

Zoback, M.D., and Zoback, M.L., 1991, Tectonic stress field of North America and relative plate motion, *in* Slemmon, B., et al., eds., The Geology of North America, Decade Map Volume 1, Neotectonics of North America: Boulder, Colorado, Geological Society of America, p. 339–366.

Zoback, M.L., 1992a, First- and second-order patterns of stress in the lithosphere: The World Stress Map Project: Journal of Geophysical Research, v. 97, no. B8, p. 11,703–11,728, doi: 10.1029/92JB00132.

Zoback, M.L., 1992b, Stress field constraints on intraplate seismicity in eastern North America: Journal of Geophysical Research, v. 97, no. B8, p. 11,761–11,782, doi: 10.1029/92JB00221.

Zoback, M.L., and Richardson, R.M., 1996, Stress perturbation associated with the Amazonas and other ancient continental rifts: Journal of Geophysical Research, v. 101, no. B3, p. 5459–5475, doi: 10.1029/95JB03256.

Zoback, M.L., and Zoback, M.D., 1980, State of stress of the conterminous United States: Journal of Geophysical Research, v. 85, no. B8, p. 6113–6156, doi: 10.1029/JB085iB11p06113.

MANUSCRIPT RECEIVED 11 JUNE 2009
REVISED MANUSCRIPT RECEIVED 7 OCTOBER 2009
MANUSCRIPT ACCEPTED 14 OCTOBER 2009

Printed in the USA

Mazzotti, S., and J. Townend, State of stress in central and eastern North America seismic zones

Supplementary Material A: Focal mechanisms for central and eastern Canada and U.S.A

zone	long.	lat.	depth	M	strike	dip	rake	event	Q	ref.
LSL	-67.810	48.710	18	4.1	317	56	53	800403	B	1
LSL	-67.210	48.990	17	4.1	189	53	65	830117	A	1
LSL	-66.450	49.610	18	3.2	231	50	83	840329	B	1
LSL	-67.510	49.310	19	3.8	187	57	66	840411	A	1
LSL	-66.350	49.610	18	3.2	201	57	66	840528	B	1
LSL	-67.600	49.260	18	3.2	319	85	-14	850816	A	1
LSL	-67.390	49.250	18	4.2	304	53	65	861109	B	1
LSL	-68.250	48.740	18	3.6	312	54	37	870503	B	2
LSL	-68.710	48.870	18	3.0	181	61	73	870617	B	2
LSL	-66.980	49.610	18	3.3	334	64	56	870806	C	2
LSL	-66.880	49.340	18	4.1	219	30	58	981022	A	4
LSL	-66.320	49.610	18	4.5	221	40	124	990316	A	19
CHV	-70.090	47.700	11	4.1	110	40	90	030613	B	20
CHV	-69.800	47.800	10	6.2	42	53	105	250301	A	13
CHV	-70.240	47.340	10	1.8	137	73	42	740609	A	2
CHV	-70.239	47.343	10	0.6	138	68	41	740609	C	9
CHV	-70.180	47.404	17	1.5	278	68	-68	740620	C	9
CHV	-70.220	47.510	15	1.5	40	45	90	740623	A	2
CHV	-70.214	47.513	15	0.4	223	44	84	740623	A	9
CHV	-69.841	47.716	16	2.0	119	60	19	740630	C	9
CHV	-70.227	47.564	4	0.2	134	69	-22	740702	C	9
CHV	-69.972	47.492	13	0.5	14	71	69	740714	C	9
CHV	-69.901	47.672	10	5.0	177	58	67	790819	B	9
CHV	-69.680	47.740	28	2.9	349	67	20	850325	B	2
CHV	-70.110	47.700	5	4.0	279	59	60	860111	A	1
CHV	-70.320	47.300	22	4.2	335	46	76	860919	B	1
CHV	-70.190	47.720	4	3.3	102	55	60	870318	A	2
CHV	-69.960	47.820	20	3.0	130	65	79	871206	A	3
CHV	-70.440	47.410	12	3.6	133	44	60	880102	B	3
CHV	-70.380	47.440	7	3.1	183	25	35	880313	A	3
CHV	-70.671	47.443	20	3.1	153	42	80	890131	A	9
CHV	-69.860	47.720	11	4.3	168	31	71	890309	A	3
CHV	-69.857	47.717	11	4.3	194	18	84	890309	C	9
CHV	-69.870	47.720	10	4.4	184	38	80	890311	A	3
CHV	-69.870	47.718	10	4.4	15	72	86	890311	C	9
CHV	-70.040	47.570	15	2.9	42	57	40	890913	C	10
CHV	-70.133	47.393	23	3.2	195	44	68	891013	B	9
CHV	-70.342	47.456	7	3.4	231	60	84	891122	A	9
CHV	-70.064	47.701	10	2.6	149	43	26	891208	C	9
CHV	-69.977	47.856	21	3.6	32	48	89	900303	A	9
CHV	-70.137	47.534	15	3.2	34	65	65	900313	A	9
CHV	-70.070	47.553	10	3.1	320	70	88	900421	C	9
CHV	-70.179	47.414	8	3.0	7	41	78	900423	C	9
CHV	-70.364	47.400	16	3.3	163	24	54	901021	A	9
CHV	-69.985	47.569	11	3.1	142	23	74	901026	C	9
CHV	-70.151	47.394	14	3.4	209	69	56	901106	D	9
CHV	-70.336	47.269	9	3.3	223	74	86	901218	C	9
CHV	-70.103	47.686	11	1.9	115	55	90	910723	C	9
CHV	-69.864	47.779	23	4.3	18	80	22	911208	B	9
CHV	-69.857	47.717	10	3.3	301	64	44	920310	C	9
CHV	-70.407	47.446	3	3.2	217	6	51	920501	C	9
CHV	-70.362	47.515	4	3.1	280	60	39	930304	A	9
CHV	-70.104	47.685	5	1.8	76	27	-62	930330	B	9
CHV	-69.889	47.668	8	3.1	165	53	72	930807	C	9
CHV	-70.361	47.453	6	3.8	116	87	24	931230	C	9
CHV	-69.660	47.770	17	4.3	37	56	90	940925	A	4
CHV	-69.961	47.752	12	4.3	37	56	90	940925	A	9

CHV	-70.314	47.437	11	3.0	70	70	-15	941201	B	9
CHV	-70.028	47.516	15	3.1	163	49	57	960512	B	9
CHV	-69.942	47.530	13	3.1	353	29	77	960607	C	9
CHV	-70.146	47.533	14	1.9	73	62	74	960617	A	9
CHV	-70.124	47.486	14	1.6	46	55	84	960624	C	9
CHV	-70.050	47.483	14	2.2	148	70	47	960714	A	9
CHV	-69.993	47.694	7	3.4	324	24	44	960714	A	9
CHV	-69.947	47.610	10	2.3	310	29	-39	960726	B	9
CHV	-70.245	47.300	6	2.1	37	22	76	960819	D	9
CHV	-70.213	47.501	12	2.2	33	75	71	960913	C	9
CHV	-69.893	47.659	14	2.2	103	79	45	960923	B	9
CHV	-70.145	47.588	21	2.0	137	33	19	960924	A	9
CHV	-70.242	47.548	13	3.1	246	67	79	960924	A	9
CHV	-69.750	47.853	22	2.2	79	69	77	960925	C	9
CHV	-70.055	47.476	16	1.9	25	29	77	961011	C	9
CHV	-70.389	47.428	4	2.2	71	50	-29	961025	A	9
CHV	-70.041	47.554	12	2.3	10	23	30	961028	A	9
CHV	-70.196	47.509	17	3.2	111	35	40	970110	A	9
CHV	-69.877	47.657	15	3.1	256	51	8	970114	C	9
CHV	-69.900	47.670	11	4.7	127	82	37	971028	A	4
NAN	-66.600	47.000	7	5.7	195	50	120	820109	A	5
NAN	-66.659	46.975	8	5.4	200	60	125	820111	B	21
NAN	-64.880	46.000	12	3.6	121	78	54	840923	B	1
NAN	-66.150	46.540	11	3.3	303	62	49	860509	B	1
NAN	-66.540	47.000	18	4.1	324	67	46	861017	A	2
NAN	-65.670	48.000	18	3.9	120	81	3	880128	B	3
NAN	-64.900	46.030	4	3.7	307	59	54	880424	A	2
NAN	-65.820	46.630	17	3.5	324	59	60	890810	C	10
NAN	-66.920	47.210	18	3.0	116	75	-85	900108	C	10
NAN	-68.230	47.290	18	3.5	145	52	71	900330	C	10
NAN	-66.600	47.000	5	4.1	343	79	33	940714	A	4
NAN	-66.610	47.020	5	4.0	131	67	112	980715	B	4
GAT	-75.090	46.230	18	4.2	117	46	76	000806	A	4
GAT	-76.360	47.010	18	4.5	155	55	59	031012	B	20
GAT	-76.280	46.460	17	4.1	296	65	80	750712	A	7
GAT	-75.030	46.090	0	3.5	308	80	-80	810918	A	8
GAT	-75.460	45.890	19	3.7	271	65	4	820806	B	8
GAT	-75.150	45.750	16	2.6	296	70	79	850130	C	8
GAT	-75.090	46.350	13	3.2	118	62	11	860605	B	1
GAT	-74.810	45.880	18	3.1	137	55	84	860618	C	1
GAT	-75.200	46.370	16	3.6	277	50	57	860806	B	1
GAT	-74.830	46.200	16	2.8	45	90	20	870521	C	2
GAT	-75.810	46.350	18	2.8	87	60	6	870707	C	2
GAT	-74.520	45.760	18	3.7	107	86	50	871023	B	2
GAT	-75.690	46.340	18	3.9	122	86	50	880310	A	2
GAT	-75.200	46.330	18	3.9	27	55	84	901007	C	10
GAT	-75.590	46.490	12	4.5	158	45	121	901019	B	19
GAT	-74.930	45.930	18	4.4	308	49	115	960314	A	4
GAT	-74.190	45.810	18	4.3	296	64	61	970524	A	4
GAT	-74.800	46.190	18	4.4	164	27	66	980730	A	4
GAT	-74.310	45.840	18	4.2	95	68	44	991031	B	4
MNT	-74.720	44.960	20	5.8	313	70	52	440905	A	17
MNT	-74.440	45.680	18	3.6	119	52	27	780730	A	8
MNT	-74.620	45.140	13	3.7	118	62	49	810704	A	8
MNT	-74.600	45.130	13	2.5	300	73	-58.0	810704	C	8
MNT	-74.610	45.120	13	1.4	280	38	-65	810705	B	8
MNT	-74.620	45.170	13	3.4	252	36	14	810705	A	8
MNT	-74.610	45.120	13	1.9	304	36	54	810707	A	8
MNT	-74.380	45.780	18	2.8	69	40	82	810920	A	8
MNT	-74.460	45.540	12	2.5	103	80	28	821031	C	8
MNT	-73.440	45.440	18	2.9	203	75	27	821124	C	8
MNT	-75.050	45.620	11	2.0	310	50	-90	831016	C	8
MNT	-73.900	45.670	18	3.4	104	61	78	831101	A	8

MNT	-74.770	45.700	11	2.8	33	42	67	831210	B	8
MNT	-75.120	45.560	19	3.0	87	51	-8	840117	B	8
MNT	-75.050	45.200	5	3.3	299	41	41	841126	A	8
MNT	-74.240	45.530	11	2.8	107	55	84	860720	C	1
MNT	-74.250	45.100	10	3.3	190	46	76	860813	A	1
MNT	-75.000	45.010	9	3.4	310	40	44	880809	A	3
MNT	-74.990	45.010	9	2.1	314	38	47	880811	A	3
MNT	-75.300	45.210	18	2.9	226	42	-50	900303	C	10
MNT	-74.960	45.580	18	4.1	313	57	53	980418	A	4
PEM	-75.750	45.200	12	4.1	224	22	63	831011	A	8
PEM	-75.750	45.200	12	1.2	52	77	59	831013	B	8
PEM	-76.680	45.610	9	3.1	272	57	66	850824	A	1
PEM	-77.340	45.780	14	3.4	317	48	19	860110	A	1
PEM	-78.420	46.310	4	3.0	178	25	-11	860530	B	1
PEM	-75.630	45.570	7	1.8	348	80	39	870619	C	2
PEM	-75.340	45.770	17	3.5	343	56	78	871111	B	2
PEM	-75.620	45.170	18	3.3	291	46	77	880515	B	3
ECA	-78.930	46.840	13	4.7	320	33	99	000101	A	19
ECA	-95.620	71.180	18	4.1	148	47	65	000405	D	4
ECA	-79.460	43.790	18	3.1	16	25	52	000524	C	4
ECA	-71.070	47.560	18	4.2	289	47	70	000712	B	4
ECA	-113.200		80.570	18	4.6	64	64	16	001003	D
4										
ECA	-116.480		80.940	18	5.2	68	55	30	001113	D
4										
ECA	-63.350	50.030	18	4.2	272	45	86	010324	B	20
ECA	-73.730	44.530	10	5.0	196	40	111	020420	A	19
ECA	-56.000	44.690	20	7.1	122	74	140	291118	A	14
ECA	-56.000	44.690	20	6.8	249	59	166	291118	A	14
ECA	-79.070	46.780	10	6.1	130	45	80	351101	A	16
ECA	-74.100	45.170	9	3.1	300	67	46	760713	B	8
ECA	-68.620	49.840	2	0.0	128	71	69	761000	A	1
ECA	-74.110	46.320	0	4.1	343	42	85	780218	A	6
ECA	-67.330	44.900	12	3.5	255	47	69	840119	B	2
ECA	-70.690	45.370	8	3.5	178	41	75	850412	A	1
ECA	-59.610	57.220	18	4.8	186	56	19	860420	A	3
ECA	-75.560	44.660	2	2.9	195	45	83	870705	B	2
ECA	-79.460	43.470	18	3.4	284	76	-74	870723	D	2
ECA	-78.890	46.850	18	3.2	284	63	72	870817	C	2
ECA	-56.330	56.720	18	4.6	222	53	56	871214	B	3
ECA	-70.820	47.030	14	3.1	296	51	77	880512	A	3
ECA	-71.200	48.130	29	4.7	343	48	82	881123	B	3
ECA	-71.210	48.130	29	6.5	326	67	55	881125	A	3
ECA	-71.180	48.120	29	5.8	170	41	139	881125	B	19
ECA	-71.300	48.140	26	4.1	339	46	103	881126	A	3
ECA	-70.100	60.050	18	5.7	260	42	58	890316	A	3
ECA	-72.640	45.920	18	2.8	66	72	64	900424	C	10
ECA	-71.170	82.180	18	4.7	80	45	-45	950308	A	4
ECA	-71.100	82.220	18	4.0	100	64	-44	950310	C	4
ECA	-59.550	61.000	18	4.2	74	80	-39	950718	C	4
ECA	-106.180		77.100	18	4.6	215	87	35	950824	B
4										
ECA	-107.180		76.670	18	4.7	71	61	29	960222	B
4										
ECA	-87.750	56.670	18	4.0	28	43	-35	960516	C	4
ECA	-76.640	59.610	18	4.2	238	49	80	970714	B	4
ECA	-71.420	46.800	22	4.5	244	35	106	971106	A	19
ECA	-88.190	64.840	18	5.7	216	73	15	971206	A	4
ECA	-54.740	59.090	18	4.9	140	43	1	980121	D	4
ECA	-91.540	76.330	18	4.1	185	53	40	980311	C	4
ECA	-56.380	43.750	18	4.4	215	40	11	980317	D	4
ECA	-79.440	81.900	18	4.3	12	74	-37	980414	B	4
ECA	-60.940	57.830	18	4.0	90	54	-20	980521	C	4

ECA	-89.890	80.970	18	5.3	137	50	2	980609	C	4
ECA	-110.240		79.790	18	5.3	85	48	19	990101	B 4
ECA	-58.030	60.900	18	5.3	117	41	-12	990729	D	4
ECA	-78.990	43.710	18	3.8	120	61	-28	991126	B	4
ECA	-120.440		75.380	18	5.7	149	77	38	991207	B 4
ECA	-70.010	73.070	10	7.3	172	82	6	331120a	A	15
ECA	-70.010	73.070	10	7.0	190	30	62	331120b	A	15
ECA	-73.600	60.120	3	5.3	251	54	46	891225a	A	12
ECA	-73.600	60.120	3	6.2	240	58	90	891225b	A	12
ECA	-73.600	60.120	3	6.3	200	85	20	891225c	A	12
CVN	-78.100	37.770	10	4.3	66	34	141	031209	A	38
CVN	-78.070	37.750	5	3.6	3	71	158	030505	U	35
CVN	-77.770	38.070	5	0.9	341	41	139	800804	C	37
CVN	-77.770	38.070	3	1.0	310	84	8	800926	C	37
CVN	-77.820	37.890	5	0.3	346	79	136	820118	C	37
CVN	-77.580	37.860	10	2.1	158	61	-8	820605	B	37
CVN	-77.500	37.840	13	1.9	316	42	129	820625	B	37
CVN	-77.500	37.840	13	1.6	327	79	17	820920	B	37
CVN	-78.420	37.750	10	1.9	333	45	-5	830810	C	37
CVN	-78.320	37.870	8	4.0	335	59	16	840817	A	37
CVN	-77.510	37.940	15	1.1	3	63	14	841017	B	37
CVN	-78.440	37.720	7	3.4	346	67	117	810211a	B	37
CVN	-78.400	37.750	10	3.2	278	35	81	810211b	C	37
WVN	-80.540	37.430	18	0.4	340	85	-178	801202	C	37
WVN	-80.510	37.390	16	1.8	340	90	145	830125	A	37
WVN	-80.320	37.510	9	2.2	82	86	-60	830526	B	37
WVN	-80.760	37.270	7	1.0	20	82	-174	830710	C	37
WVN	-80.790	37.200	12	1.1	303	76	27	830912	B	37
WVN	-80.720	37.290	11	1.4	207	66	-147	840207	B	37
NMA	-88.990	36.890	5	4.0	165	85	15	030606	C	35
NMA	-89.680	36.730	2	3.5	175	55	70	040615	B	35
NMA	-90.230	35.750	14	4.1	55	80	-165	050210	A	35
NMA	-90.150	35.830	8	4.2	315	60	20	050501	B	35
NMA	-89.460	36.140	15	3.9	155	65	70	050602	B	35
NMA	-88.960	36.950	4	3.6	320	80	15	050620	A	35
NMA	-89.510	36.370	8	4.2	350	84	145	620202	A	29
NMA	-90.050	36.640	15	4.7	304	78	-28	630303	B	28
NMA	-89.310	37.220	2	3.6	280	70	-20	650814	B	29
NMA	-89.950	35.860	16	4.1	220	75	150	701117	A	29
NMA	-89.680	36.540	9	3.7	85	60	-20	750613	A	29
NMA	-90.480	35.590	16	4.2	45	80	-150	760325	A	29
NMA	-90.480	35.590	12	4.6	220	65	150	760325	A	29
NMA	-89.580	37.160	15	4.3	140	75	50	900926	B	28
NMA	-89.830	36.560	8	4.1	90	67.5	20	910504	A	28
NMA	-89.190	37.360	16	3.9	30	70	170	940205	A	28
NMA	-90.000	35.970	11	3.8	120	65	-15	961129	A	35
NMA	-89.160	36.860	5	3.5	140	70	20	040716a	B	35
ETN	-84.160	35.550	14	3.4	90	53	-16	830708	C	36
ETN	-83.710	36.120	11	3.6	83	80	-2	840214	B	36
ETN	-84.030	35.840	2	3.0	93	85	-29	840317	C	36
ETN	-85.510	35.200	27	3.0	268	40	-26	840419	B	36
ETN	-84.350	35.560	17	3.2	284	56	23	840830	A	36
ETN	-85.210	34.760	18	4.0	90	41	-11	841009	B	36
ETN	-83.710	35.700	13	3.3	63	79	-44	851222	A	36
ETN	-84.750	35.610	22	3.1	254	76	-32	860107	A	36
ETN	-84.500	35.450	19	2.5	256	85	-70	860602	A	36
ETN	-84.990	34.940	13	3.8	109	85	-30	860711	B	36
ETN	-84.190	36.340	13	2.8	283	51	8	870222	C	36
ETN	-84.230	35.570	19	4.2	275	83	45	870327	A	36
ETN	-84.230	35.570	18	2.7	92	80	-18	870409	B	36
ETN	-83.820	36.100	25	3.7	307	55	-4	870711	B	36

ETN	-83.820	36.110	23	3.2	302	59	-16	870711	B	36
ETN	-84.400	35.520	20	3.1	268	41	-12	870901	B	36
ETN	-84.320	35.630	20	3.3	96	71	-30	870922	B	36
ETN	-84.190	35.280	13	2.9	300	62	-22	880109	B	36
ETN	-84.670	35.360	10	2.5	59	48	-19	880213	C	36
ETN	-83.820	35.330	1	3.5	332	50	23	880218	B	36
ETN	-83.990	35.820	14	2.4	290	83	-19	880311	C	36
ETN	-84.210	35.780	18	2.3	261	55	-30	880423	B	36
ETN	-83.740	36.110	17	2.3	111	79	-49	880424	A	36
ETN	-84.430	35.500	23	2.9	266	73	-58	890907	B	36
ETN	-83.930	36.610	25	2.4	113	71	-36	891202	B	36
ETN	-85.020	35.050	4	3.1	227	76	-27	930115	B	36
CHL	-80.178	32.963	7	2.3	300	70	19	810319	B	39
CHL	-80.167	32.935	7	3.3	321	78	52	831106	B	39
CHL	-80.146	32.941	5	1.9	357	49	121	871006	B	39
CHL	-80.148	32.934	6	3.3	276	35	36	880123	A	39
CHL	-80.218	32.979	10	2.0	7	49	119	880623	C	39
CHL	-80.158	32.929	7	2.0	325	40	90	890602	A	39
CHL	-80.155	32.930	7	1.6	350	90	175	890608	A	39
CHL	-80.152	32.949	5	2.8	13	52	161	900618	B	39
CHL	-80.140	32.932	6	2.7	347	77	113	900818	C	39
CHL	-80.130	32.945	4	3.4	10	56	110	901113	C	39
CHL	-80.152	32.987	6	1.5	15	45	115	910824	B	39
EUS	-78.900	46.870	10	4.6	116	68	69	000101	U	25
EUS	-74.250	43.950	6	3.6	150	54	120	000420	U	25
EUS	-80.830	41.990	5	3.9	5	79	159	010126	U	25
EUS	-92.190	35.190	5	4.3	20	85	-165	010504	U	35
EUS	-104.640		37.150	3	4.2	215	30	-80	010904	U 35
EUS	-104.470		37.140	2	4.4	190	25	-130	010905	U 35
EUS	-73.660	44.510	10	5.0	360	35	80	020420	U	35
EUS	-87.780	37.970	19	4.5	120	80	10	020618	U	35
EUS	-98.900	42.810	8	4.1	90	50	-110	021103	U	35
EUS	-80.070	32.360	9	4.0	350	40	90	021111	U	35
EUS	-85.500	34.550	12	4.6	275	75	5	030429	U	35
EUS	-85.500	34.550	12	4.6	275	75	5	030429	U	35
EUS	-101.750		43.100	15	3.9	85	60	-130	030525	U 35
EUS	-91.720	36.800	5	3.7	25	80	-165	030816	U	35
EUS	-104.990		36.850	4	4.1	170	55	-100	030913	U 35
EUS	-104.850		36.850	4	4.4	175	55	-95	040322	U 35
EUS	-104.560		32.530	3	3.9	345	50	-120	040523	U 35
EUS	-104.580		32.530	2	3.6	5	70	-110	040622	U 35
EUS	-88.960	41.440	7	4.2	20	90	-165	040628	U	35
EUS	-104.920		36.890	4	4.3	155	65	-120	040801	U 35
EUS	-78.250	43.690	3	3.2	125	65	35	040804	U	35
EUS	-86.280	64.760	23	4.2	155	60	80	040826	U	35
EUS	-85.750	39.610	13	3.8	320	75	15	040912	U	35
EUS	-87.900	32.970	3	4.3	35	40	-115	041107	U	35
EUS	-69.730	47.750	12	4.6	350	30	80	050306	U	35
EUS	-104.860		36.950	4	4.9	160	40	-110	050810	U 35
EUS	-82.800	35.880	8	3.7	90	60	-60	050825	U	35
EUS	-104.570		32.520	5	4.1	230	40	-85	051219	U 35
EUS	-70.460	47.380	25	3.8	15	55	85	060407	U	35
EUS	-68.790	47.000	17	3.5	170	25	45	060714	U	35

EUS	-68.170	44.330	2	3.9	340	35	85	061003	U	35
EUS	-104.900	37.060	2	4.4	205	50	-60	070103	U	35
EUS	-96.270	22.020	11	5.6	190	75	-160	070523	U	35
EUS	-104.790	36.930	4	3.4	195	50	-60	070609	U	35
EUS	-90.940	37.480	5	4.6	260	40	-70	651021	A	29
EUS	-78.200	42.800	2	4.3	110	70	20	660101	A	29
EUS	-104.800	39.900	4	4.5	165	52	-174	670410	U	22
EUS	-78.200	42.900	3	4.1	130	50	40	670613	A	29
EUS	-90.440	37.440	15	4.0	350	60	135	670721	B	28
EUS	-104.700	39.900	3	4.8	130	35	-90	670809	U	22
EUS	-104.700	40.000	5	4.5	158	52	-63	671127	U	22
EUS	-88.370	37.910	22	5.3	0	46	79	681109	A	29
EUS	-86.500	64.400	12	4.6	162	72	90	711002	A	29
EUS	-80.580	33.310	2	4.4	260	40	10	720203	U	24
EUS	-82.530	33.910	2	4.0	350	65	100	720802	U	24
EUS	-89.400	41.600	13	4.1	170	70	160	720915	B	29
EUS	-70.900	45.300	6	4.5	300	80	70	730615	A	29
EUS	-84.000	35.800	13	4.1	190	70	150	731130	C	29
EUS	-88.070	38.550	15	4.3	310	70	0	740403	B	29
EUS	-96.000	45.700	8	4.3	330	90	160	750709	B	29
EUS	-100.700	33.000	3	4.5	260	60	-60	780616	U	28
EUS	-83.910	38.170	12	5.0	30	60	180	800727	U	23
EUS	-66.650	46.980	7	5.1	200	60	125	820111	U	21
EUS	-71.600	43.500	8	4.2	200	35	120	820119	U	21
EUS	-92.210	35.170	6	5.0	330	60	55	820121	U	21
EUS	-74.260	43.940	9	4.9	170	70	115	831007	U	21
EUS	-105.720	42.370	25	5.3	350	60	335	841018	U	21
EUS	-81.160	41.650	6	4.7	25	80	165	860131	U	21
EUS	-84.390	40.550	4	4.4	20	80	-170	860712	U	30
EUS	-87.950	38.710	10	5.0	135	70	15	870610	U	31
EUS	-75.590	46.470	11	4.6	141	42	90	901019	U	25
EUS	-73.460	45.200	12	3.9	144	45	96	931116	U	25
EUS	-103.300	30.260	20	5.6	114	64	-101	950414	U	26
EUS	-71.910	44.290	6	3.7	95	50	40	950616	U	25
EUS	-74.430	45.990	6	3.7	136	36	98	960314	U	25
EUS	-71.350	44.180	7	3.4	144	60	93	960821	U	25
EUS	-74.190	45.810	22	3.6	96	33	60	970524	U	25
EUS	-87.300	31.200	5	4.9	94	62	-90	971024	U	35
EUS	-69.910	47.670	5	4.3	27	66	111	971028	U	25
EUS	-71.350	46.750	12	4.5	39	63	87	971106	U	25
EUS	-98.510	34.940	19	3.9	120	70	-60	980428	U	35
EUS	-74.720	46.170	9	3.7	150	27	75	980730	U	25
EUS	-80.390	41.490	3	4.5	110	70	20	980925	U	34
EUS	-66.390	49.690	5	4.4	30	63	93	990316	U	25
EUS	-95.560	40.630	12	3.5	290	55	-135	040716b	U	35
EUS	-86.930	33.180	4	3.6	30	30	-100	040819b	U	35
EUS	-66.660	46.980	9	5.5	200	45	120	820109a	U	21
EUS	-66.650	47.020	6	4.8	215	60	130	820109b	U	21
EUS	-76.010	40.340	2	4.0	156	45	108	940116a	U	25
EUS	-76.010	40.340	3	4.0	121	60	66	940116a	U	33
EUS	-76.050	40.340	2	4.6	159	48	102	940116b	U	25
EUS	-76.050	40.340	3	4.6	135	49	68	940116b	U	33

zone: seismic zone – ECA: Eastern Canada; EUS: Eastern U.S.A.; LSL: Lower St.

Lawrence; CHV: Charlevoix; GAT: Gatineau; MNT: Montreal; NAN: North Appalachian; OTT: Ottawa Valley; CVN: Central Virginia; ETN: Eastern Tennessee; NMA: New Madrid; CHL: Charleston.

long., lat., depth: longitude (°E), latitude (°N) and depth (km) of epicenter.

M: earthquake magnitude (magnitude scale vary between events, cf. individual references).

strike, dip, rake: angle (°) of strike, dip, and rake of one of the two fault planes.

event: earthquake number defined as year, month, day (YYMMDD).

Q: quality factor of focal mechanism: A (highest) to C (lowest); U: undefined.

ref.: reference:
1 - Adams, J., J. Sharp, and M.C. Stagg, 1988, New focal mechanisms for southeastern Canadian earthquakes, Geol. Surv. Canada Open File, OF1892, p. 112.
2 - Adams, J., A. Vonk, D. Pittman, and H. Vatcher, 1989, New focal mechanisms for southeastern Canadian earthquakes II, Geol. Surv. Canada Open File, OF1995, p. 97.
3 - Adams, J., 1991, New focal mechanisms for eastern Canada, Geol. Surv. Canada Open File, OF2430, p. 118.
4 - Bent, A. L., J. Drysdale, and H. K. C. Perry, 2003, Focal mechanisms for eastern Canadian earthquakes: 1994-2000, Seism. Res. Lett., 74, 452-468.
5 - Wetmiller, R. J., J. Adams, F. M. anglin, H. S. Hasegawa, and A. E. Stevens,1 984, Aftershock sequences of the 1982 Miramichi, New Brunswick, earthquakes, Bull. Seism. Soc. Amer., 74, 621-653.
6 - Horner, R. B., Wetmiller, R. J., and H. S. Hasegawa, 1979, The St-Donat, Quebec, earthquake sequence of February 18-23, 1978, Can. J. Earth. Sci., 16, 1892-1898.
7 - Horner, R. B., Stevens, A. E., Hasegawa, H. S., and G. LeBlanc, 1978, Focal parameters of the July 12, 1975, Maniwaki, Quebec, Earthquake _ An example of intraplate seismicity in eastern Canada, Bull.. Seism. Soc. Amer., 68, 619-640.
8 - Wahlstrom, R., 1987, Focal mechanisms of earthquakes in southern Quebec, southeastern Ontario, and northeastern New York with implications for regional seismotectonics and stress field characteristics, Bull. Seism. Soc. Amer., 77, 891-924.
9 - Lamontagne, M., 1998, New and revised earthquake focal mechanisms for the Charlevoix seismic zone, Canada, Geol. Surv. Canada Open File, OF3556, p. 302.
10 - Seismological Service, Canadian Earthquakes National Summary, Natural Resources Canada, 1989-1990.
11 - Lamontagne, M., H. S. Hasegawa, D. A. Forsyth, G. G. R. Buchbinder, and M. Cajka , 1994, The Mont-Laurier, Quebec, earthquake of 19 October 1990 and its seismotectonic environment, Bull. Seism. Soc. Amer., 84, 1506-1522.
12 - Bent, A. L., 1994, The 1989 (Ms 6.3) Ungava, Quebec, Earthquake: a complex intraplate event, Bull. Seism. Soc. Amer., 84, 1075-1088.
13 - Bent, A. L., 1992, A re-examination of the 1925 Charlevoix, Quebec, earthquake, Bull. Seism. Soc. Amer., 82, 2097-2113.
14 - Bent, A. L., 1995, A complex double-couple source mechanism for the Ms 7.2 1929 Grand Banks earthquake, Bull. Seism. Soc. Amer., 85, 1003-1020.
15 - Bent, A. L., 2002, The 1933 Ms=7.3 Baffin Bay earthquake: strike-slip faulting along the northeastern Canadian passive margin, Geophys. J. Int., 150, 724-736.
16 - Bent, A. L., 1996, An improved source mechanism for the 1935 Timiskaming, Quebec, earthquake from regional waveforms, Pure Applied Geophys., 146, 1-20.
17 - Bent, A. L., 1996, Source parameters of the damaging Cornwall-Massena earthquake of 1944 from regional waveforms, Bull. Seism. Soc. Amer., 86, 489-497.
18 - Lamontagne, M., A. L. Bent, C. R. D. Woodgold, S. Ma, V. Peci, 2004, The 16 March 1999 mn 5.1 Cote-Nord earthquake: the largest earthquake ever recorded in the lower St. Lawrence seismic zone, Canada, Seism. Res. Lett., 75, 299-313.
19 - Ma, S., 2004, Personal communication.
20 - Bent, A. L., 2004, Personal communication.
21 - Nguyen, B. V., and R. B. Herrmann, 1992, Determination of source parameters for central and eastern North America earthquakes (1982-1986), Seism. Res. Lett., 63,

567-577.
22 - Herrmann, R. B., C. Y. Wang, and S. -K. Park, 1981, The Denver earthquakes of 1967-1968, Bull. Seism. Soc. Am., 71, 731-746.
23 - Herrmann, R. B., C. A. Langston, and J. E. Zollweg, 1982, The Sharpsburg, Kentucky earthquake of July 27, 1980, Bull. Seism. Soc. Am., 72, 1219-1239.
24 - Herrmann, R. B., 1986, Surface-wave studies of some South Carolina earthquakes, Bull. Seism. Soc. Am., 76, 111-121.
25 - Du, W.X., W.Y. Kim, and L. R. Sykes, 2003, Earthquake Source Parameters and State of Stress for the Northeastern United States and Southeastern Canada from Analysis of Regional Seismograms, Bull. Seism. Soc. Am., 93, 1633-1648.
26 - Chang, T.M., 1997, Evaluation of Surface-Wave Waveform Modeling for Lithosphere Velocity Structure, Ph.D. Dissertation, Saint Louis University.
27 - Voss, J. A., and R. B. Herrmann, 1980, A surface wave study of the June 16, 1978 Texas earthquake, Earthquake Notes, 51, 3-14.
28 - Herrmann, R. B., and C. J. Ammon, 1997, Faulting parameters of earthquakes in the New Madrid, Missouri region, Enginer. Geol., 46, 299-311.
29 - Herrmann, R. B., 1979, Surface wave focal mechanisms for eastern North American earthquakes with tectonic implications, J. Geophys. Res., 84, 3543-3552.
30 - Schwartz, S. Y., and D. H. Christensen, 1988, The 12 July St. Marys, Ohio earthquake and recent seismicity in the Anna, Ohio seismogenic zone, Seism. Res. Lett., 59, 57-62.
31 - Taylor, K. B., R. B. Herrmann, M. W. Hamburger, G. L. Pavlis, A. Johnston, C. Langer and C. Lam, 1989, The southeastern Illinois earthquake of 10 June 1987, Seism. Res. Lett., 60, 101-110.
32 - Nguyen, B. V., and R. B. Herrmann, 1992, Determination of source parameters for central and eastern North American earthquakes (1982-1986), Seism. Res. Lett., 63, 567-586.
33 - Ammon, C. J., R. B. Herrmann, C. A. Langston, and H. Benz, 1998, Source parameters of the January 16, 1994 Wyomissing Hills, Pennsylvania earthquakes, Seism. Res. Lett., 69, 261-269.
34 - Maceira, M., C. J. Ammon and R. B. Herrmann, 2000, Faulting parameters of the September 25, 1998 Pymatuning, Pennsylvania earthquake, Seism. Res. Lett., 71, 742-752.
35 – Moment Tensor Solutions, Saint Louis Univ., Dep. Earth Atm. Sci., web site; http://www.eas.slu.edu/Earthquake_Center/MECH.NA/index.html.
36 - Chapman, M. C., C. A. Powel, G. Vlahovic, and M. S. Sibol, 1997, A statistical analysis of earthquake focal mechanisms and epicenter locations in the Eastern Tennessee seismic zone, Bull. Seism. Soc. Am., 87, 1522-1536.
37 - Munsey, J.W., and G.A. Bollinger, 1985, Focal mechanism analyses for Virginia earthquakes, Bull. Seism. Soc. Amer., 75, 1613-1636.
38 - Kim, W.Y., and M. Chapman, The 9 December 2003 central Virginia earthquake sequence: A compound earthquake in the Central Virginia seismic zone, Bull. Seism. Soc. Amer., 95, 2428-2445.
39 - Madabhushi, S., and P. Talwani, 1993, Fault plane solutions and relocations of recent earthquakes in Middleton Place Summerville seismic zone near Charleston, South Carolina, Bull. Seism. Soc. Amer., 83, 1442-1466.

Mazzotti, S., and J. Townend, State of stress in central and eastern North America seismic zones

Supplementary Material B: Octant plots of focal mechanisms

This supplement presents octant plots of the focal mechanisms used for the stress inversion in each seismic zone (Fig. B1). The octant plots (also called eigenvector representation) are based on the formulation developed in Kagan (2005). As shown in Figure B1, the diversity of mechanisms varies signicantly between seismic zones. Zones such as Lower St. Lawrence or Ottawa are characterized by mechanisms that are mostly similar (mainly reverse-fault mechanisms in those two cases). In contrast, zones such as Montreal or Charlevoix show higher diversity with mechanisms varying between reverse, strike-slip, and normal faulting.

Figure B1: Octant plots of focal mechanisms in central and eastern North America seismic zones. Grey triangles represent individual focal mechanisms. Plunge angles of 30° and 60° shown by thin solid lines. Boundaries between strike-slip, normal and reverse faulting shown by dashed lines. RF: reverse fault; NF: normal fault; SS: strike-slip.

References

Kagan, Y. Y., 2005, Double-couple earthquake focal mechanisms: random rotation and display, Geophys. J. Int., 163, 1065-1072.

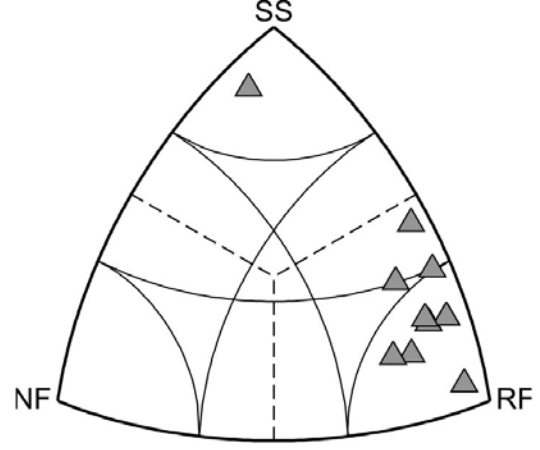

Lower St. Lawrence

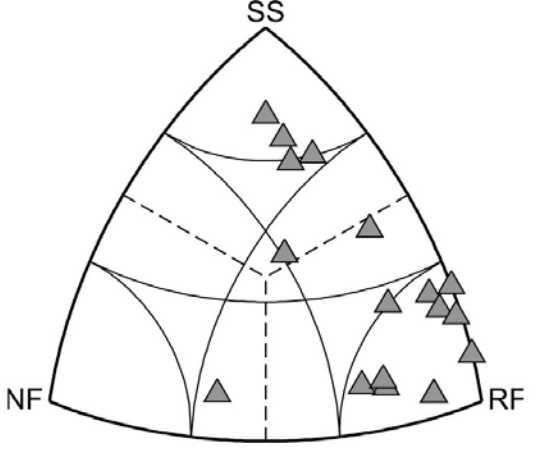

Gatineau

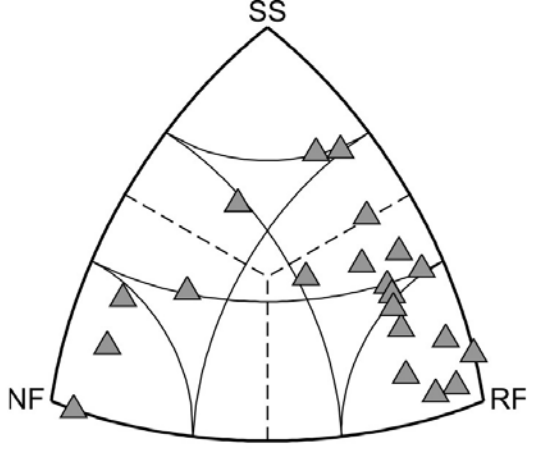

Montreal

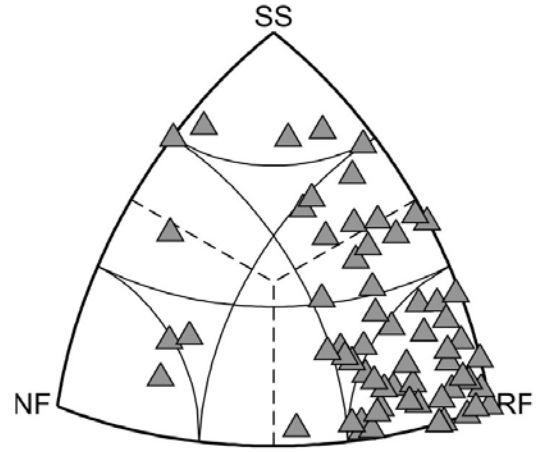

Charlevoix

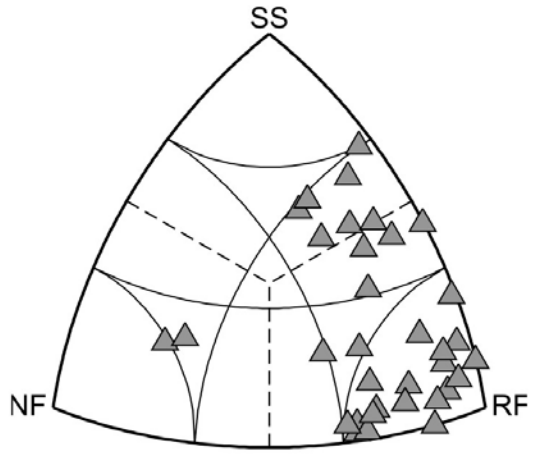

Charlevoix - SE

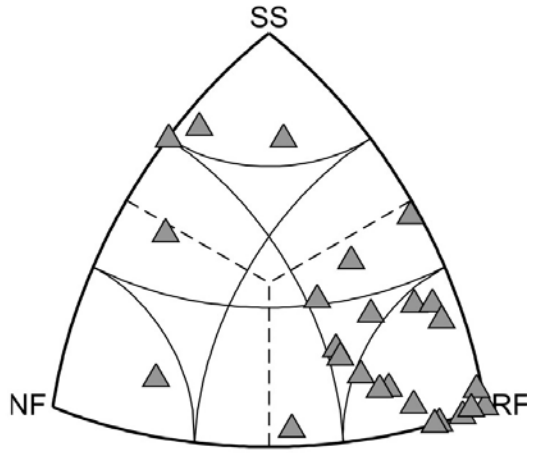

Charlevoix - NW

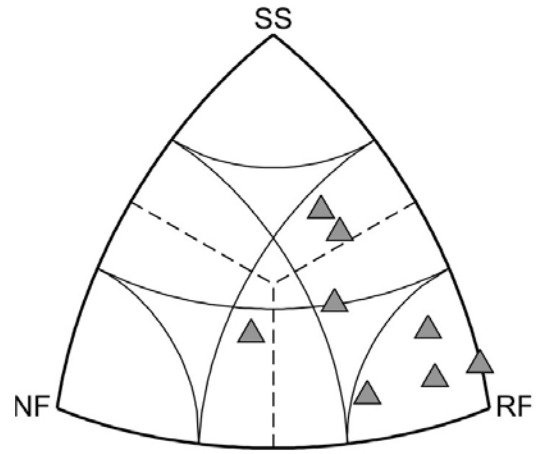

Ottawa

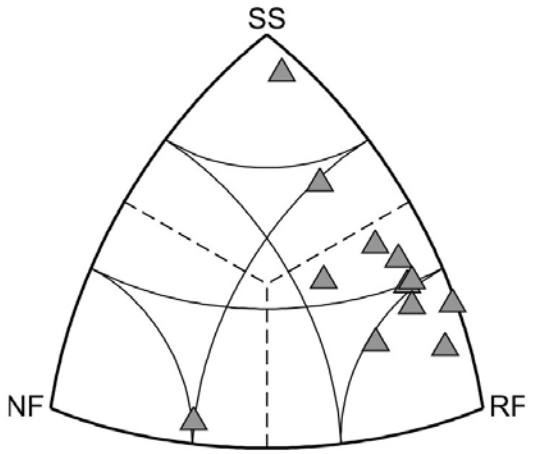

North Appalachian

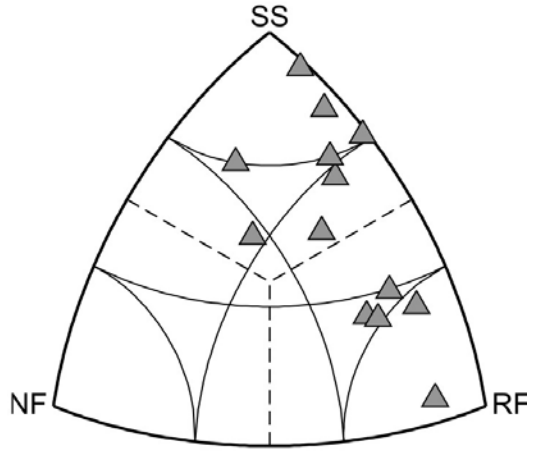

Central Virginia

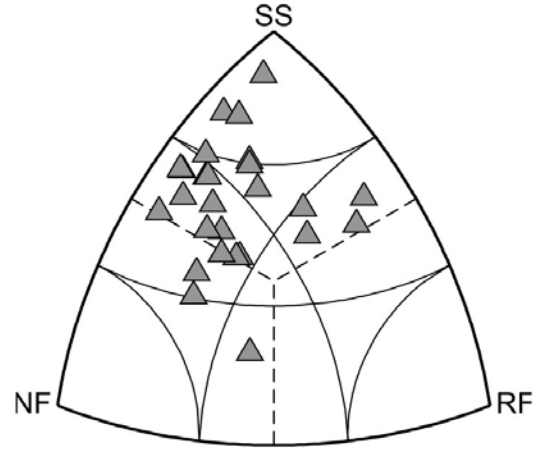

Eastern Tennessee

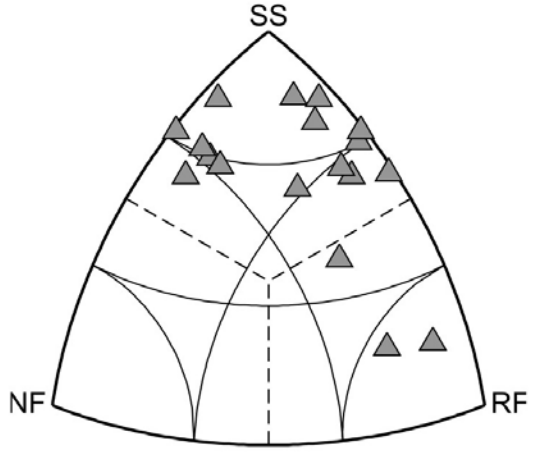

New Madrid

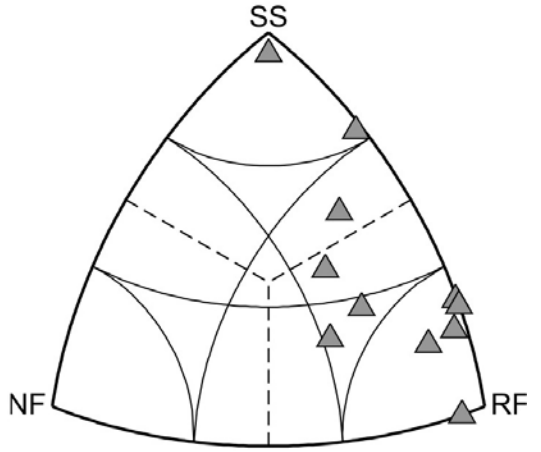

Charleston

Mazzotti, S., and J. Townend, State of stress in central and eastern North America seismic zones

Supplementary Material C: Stress inversions for groups of mechanisms in the Charlevoix seismic zone

This supplement presents the results of inversion tests for various groups of earthquake focal mechanisms in the Charlevoix seismic zone (Fig. C1): Inside and outside the inner perimeter of impact crater (1a, b), inside and outside the outer perimeter of impact crater (2a, b), northern cluster (3), southeast central cluster (4), northwest central cluster (5), southern cluster (6), northern half (7), southern half (8), entire dataset (9), southeast (10 and northwest (11) clusters (cf. Section 4.4).

Groups of mechanisms located entirely or mainly to the northwest of the Charlevoix Fault (1a, 5 and 6, Table C1) are associated with a SH azimuth about N050-060°, similar to the orientation obtained for the northwest group (11, Table C1). Groups of mechanisms located entirely or mainly to the southeast of the Charlevoix fault (4, Table C1) or at the northern end of the seismic zone (2b and 3, Table C1) are associated with a SH azimuth about N100-120°, similar to the orientation obtained for the southeast group (10, Table C1). Other groups, which include mechanisms located roughly evenly across the Charlevoix Fault (1b, 2a, 7 and 8, Table C1), are associated with an intermediate SH azimuth of about N070-090°.

There is no clear indication of significant variations in SH orientation inside versus outside the impact crater or as a function of depth. A previously postulated SH rotation with depth (Adams and Bell, 1991) is likely an artifact arising from the heterogeneous lateral distribution of earthquakes within depth slices. Observed rotations for these groups are related to the location of mechanisms primarily to the southeast or northwest of the Charlevoix seismic zone (e.g., 2b, Table C1).

Table C1. Maximum horizontal stress median orientation (SH) and 90% confidence interval (90CIH) for various groups.

Sub-group	N	SH (°)	90CIH (°)
1a - Small crater - inside	21	52	39 – 65
1b - Small crater - outside	44	81	92 – 103
2a - Large crater - inside	42	68	59 – 78
2b - Large crater - outside	21	107	90 – 119
3 - Northern cluster	16	124	58 – 144
4 - SE central cluster	15	112	86 – 136
5 - NW central cluster	15	55	36 – 73
6 - Southern cluster	8	59	41 – 76
7 – Northern half	27	88	70 – 102
8 – Southern half	38	71	60 – 82
9 - All	65	59	41 – 76
10 - South-east	35	98	85 – 111
11 - North-west	25	57	46 – 68

Figure C1: Locations of focal mechanism groups for the Charlevoix seismic zone. Large grey circles show epicenters of focal mechanism events. Numbers refer to groups (cf. text). Small and large dashed circles show extent of inner and outer perimeter of Charlevoix impact crater.

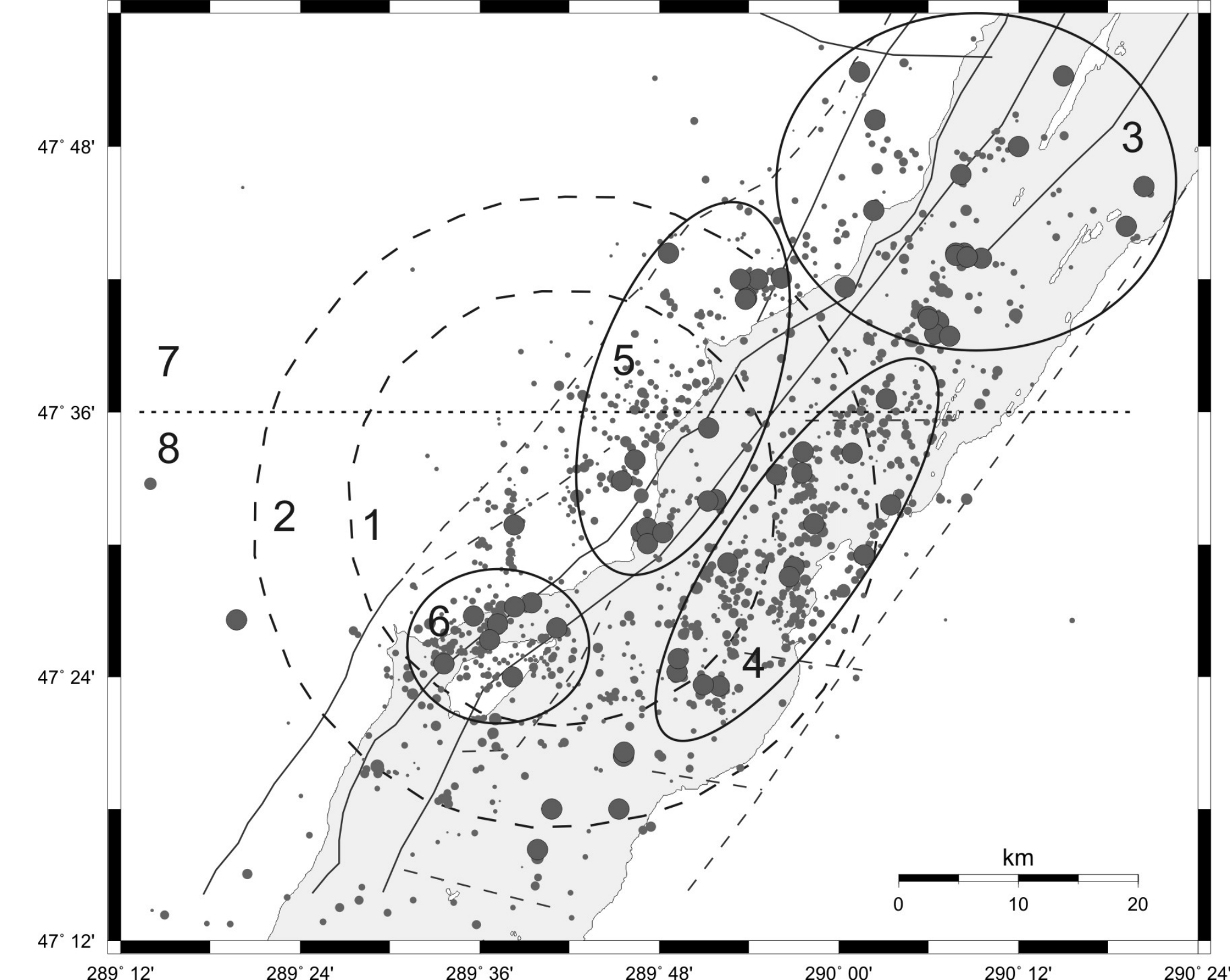
47° 48'
47° 36'
47° 24'
47° 12'
289° 12'
289° 24'
289° 36'
289° 48'
290° 00'
290° 12'
290° 24'
1
2
3
4
5
6
7
8
km
0
10
20

zone	long.	lat.	depth	M	strike	dip	rake	event	Q	ref.
LSL	-67.810	48.710	18	4.1	317	56	53	800403	B	1
LSL	-67.210	48.990	17	4.1	189	53	65	830117	A	1
LSL	-66.450	49.610	18	3.2	231	50	83	840329	B	1
LSL	-67.510	49.310	19	3.8	187	57	66	840411	A	1
LSL	-66.350	49.610	18	3.2	201	57	66	840528	B	1
LSL	-67.600	49.260	18	3.2	319	85	-14	850816	A	1
LSL	-67.390	49.250	18	4.2	304	53	65	861109	B	1
LSL	-68.250	48.740	18	3.6	312	54	37	870503	B	2
LSL	-68.710	48.870	18	3.0	181	61	73	870617	B	2
LSL	-66.980	49.610	18	3.3	334	64	56	870806	C	2
LSL	-66.880	49.340	18	4.1	219	30	58	981022	A	4
LSL	-66.320	49.610	18	4.5	221	40	124	990316	A	19
CHV	-70.090	47.700	11	4.1	110	40	90	030613	B	20
CHV	-69.800	47.800	10	6.2	42	53	105	250301	A	13
CHV	-70.240	47.340	10	1.8	137	73	42	740609	A	2
CHV	-70.239	47.343	10	0.6	138	68	41	740609	C	9
CHV	-70.180	47.404	17	1.5	278	68	-68	740620	C	9
CHV	-70.220	47.510	15	1.5	40	45	90	740623	A	2
CHV	-70.214	47.513	15	0.4	223	44	84	740623	A	9
CHV	-69.841	47.716	16	2.0	119	60	19	740630	C	9
CHV	-70.227	47.564	4	0.2	134	69	-22	740702	C	9
CHV	-69.972	47.492	13	0.5	14	71	69	740714	C	9
CHV	-69.901	47.672	10	5.0	177	58	67	790819	B	9
CHV	-69.680	47.740	28	2.9	349	67	20	850325	B	2
CHV	-70.110	47.700	5	4.0	279	59	60	860111	A	1
CHV	-70.320	47.300	22	4.2	335	46	76	860919	B	1
CHV	-70.190	47.720	4	3.3	102	55	60	870318	A	2
CHV	-69.960	47.820	20	3.0	130	65	79	871206	A	3
CHV	-70.440	47.410	12	3.6	133	44	60	880102	B	3
CHV	-70.380	47.440	7	3.1	183	25	35	880313	A	3
CHV	-70.671	47.443	20	3.1	153	42	80	890131	A	9
CHV	-69.860	47.720	11	4.3	168	31	71	890309	A	3
CHV	-69.857	47.717	11	4.3	194	18	84	890309	C	9
CHV	-69.870	47.720	10	4.4	184	38	80	890311	A	3
CHV	-69.870	47.718	10	4.4	15	72	86	890311	C	9
CHV	-70.040	47.570	15	2.9	42	57	40	890913	C	10
CHV	-70.133	47.393	23	3.2	195	44	68	891013	B	9
CHV	-70.342	47.456	7	3.4	231	60	84	891122	A	9
CHV	-70.064	47.701	10	2.6	149	43	26	891208	C	9
CHV	-69.977	47.856	21	3.6	32	48	89	900303	A	9
CHV	-70.137	47.534	15	3.2	34	65	65	900313	A	9
CHV	-70.070	47.553	10	3.1	320	70	88	900421	C	9
CHV	-70.179	47.414	8	3.0	7	41	78	900423	C	9
CHV	-70.364	47.400	16	3.3	163	24	54	901021	A	9
CHV	-69.985	47.569	11	3.1	142	23	74	901026	C	9
CHV	-70.151	47.394	14	3.4	209	69	56	901106	D	9
CHV	-70.336	47.269	9	3.3	223	74	86	901218	C	9
CHV	-70.103	47.686	11	1.9	115	55	90	910723	C	9
CHV	-69.864	47.779	23	4.3	18	80	22	911208	B	9
CHV	-69.857	47.717	10	3.3	301	64	44	920310	C	9
CHV	-70.407	47.446	3	3.2	217	6	51	920501	C	9
CHV	-70.362	47.515	4	3.1	280	60	39	930304	A	9
CHV	-70.104	47.685	5	1.8	76	27	-62	930330	B	9
CHV	-69.889	47.668	8	3.1	165	53	72	930807	C	9
CHV	-70.361	47.453	6	3.8	116	87	24	931230	C	9
CHV	-69.660	47.770	17	4.3	37	56	90	940925	A	4
CHV	-69.961	47.752	12	4.3	37	56	90	940925	A	9
CHV	-70.314	47.437	11	3.0	70	70	-15	941201	B	9
CHV	-70.028	47.516	15	3.1	163	49	57	960512	B	9
CHV	-69.942	47.530	13	3.1	353	29	77	960607	C	9
CHV	-70.146	47.533	14	1.9	73	62	74	960617	A	9
CHV	-70.124	47.486	14	1.6	46	55	84	960624	C	9

CHV	-70.050	47.483	14	2.2	148	70	47	960714	A	9
CHV	-69.993	47.694	7	3.4	324	24	44	960714	A	9
CHV	-69.947	47.610	10	2.3	310	29	-39	960726	B	9
CHV	-70.245	47.300	6	2.1	37	22	76	960819	D	9
CHV	-70.213	47.501	12	2.2	33	75	71	960913	C	9
CHV	-69.893	47.659	14	2.2	103	79	45	960923	B	9
CHV	-70.145	47.588	21	2.0	137	33	19	960924	A	9
CHV	-70.242	47.548	13	3.1	246	67	79	960924	A	9
CHV	-69.750	47.853	22	2.2	79	69	77	960925	C	9
CHV	-70.055	47.476	16	1.9	25	29	77	961011	C	9
CHV	-70.389	47.428	4	2.2	71	50	-29	961025	A	9
CHV	-70.041	47.554	12	2.3	10	23	30	961028	A	9
CHV	-70.196	47.509	17	3.2	111	35	40	970110	A	9
CHV	-69.877	47.657	15	3.1	256	51	8	970114	C	9
CHV	-69.900	47.670	11	4.7	127	82	37	971028	A	4
NAN	-66.600	47.000	7	5.7	195	50	120	820109	A	5
NAN	-66.659	46.975	8	5.4	200	60	125	820111	B	21
NAN	-64.880	46.000	12	3.6	121	78	54	840923	B	1
NAN	-66.150	46.540	11	3.3	303	62	49	860509	B	1
NAN	-66.540	47.000	18	4.1	324	67	46	861017	A	2
NAN	-65.670	48.000	18	3.9	120	81	3	880128	B	3
NAN	-64.900	46.030	4	3.7	307	59	54	880424	A	2
NAN	-65.820	46.630	17	3.5	324	59	60	890810	C	10
NAN	-66.920	47.210	18	3.0	116	75	-85	900108	C	10
NAN	-68.230	47.290	18	3.5	145	52	71	900330	C	10
NAN	-66.600	47.000	5	4.1	343	79	33	940714	A	4
NAN	-66.610	47.020	5	4.0	131	67	112	980715	B	4
GAT	-75.090	46.230	18	4.2	117	46	76	000806	A	4
GAT	-76.360	47.010	18	4.5	155	55	59	031012	B	20
GAT	-76.280	46.460	17	4.1	296	65	80	750712	A	7
GAT	-75.030	46.090	0	3.5	308	80	-80	810918	A	8
GAT	-75.460	45.890	19	3.7	271	65	4	820806	B	8
GAT	-75.150	45.750	16	2.6	296	70	79	850130	C	8
GAT	-75.090	46.350	13	3.2	118	62	11	860605	B	1
GAT	-74.810	45.880	18	3.1	137	55	84	860618	C	1
GAT	-75.200	46.370	16	3.6	277	50	57	860806	B	1
GAT	-74.830	46.200	16	2.8	45	90	20	870521	C	2
GAT	-75.810	46.350	18	2.8	87	60	6	870707	C	2
GAT	-74.520	45.760	18	3.7	107	86	50	871023	B	2
GAT	-75.690	46.340	18	3.9	122	86	50	880310	A	2
GAT	-75.200	46.330	18	3.9	27	55	84	901007	C	10
GAT	-75.590	46.490	12	4.5	158	45	121	901019	B	19
GAT	-74.930	45.930	18	4.4	308	49	115	960314	A	4
GAT	-74.190	45.810	18	4.3	296	64	61	970524	A	4
GAT	-74.800	46.190	18	4.4	164	27	66	980730	A	4
GAT	-74.310	45.840	18	4.2	95	68	44	991031	B	4
MNT	-74.720	44.960	20	5.8	313	70	52	440905	A	17
MNT	-74.440	45.680	18	3.6	119	52	27	780730	A	8
MNT	-74.620	45.140	13	3.7	118	62	49	810704	A	8
MNT	-74.600	45.130	13	2.5	300	73	-58.0	810704	C	8
MNT	-74.610	45.120	13	1.4	280	38	-65	810705	B	8
MNT	-74.620	45.170	13	3.4	252	36	14	810705	A	8
MNT	-74.610	45.120	13	1.9	304	36	54	810707	A	8
MNT	-74.380	45.780	18	2.8	69	40	82	810920	A	8
MNT	-74.460	45.540	12	2.5	103	80	28	821031	C	8
MNT	-73.440	45.440	18	2.9	203	75	27	821124	C	8
MNT	-75.050	45.620	11	2.0	310	50	-90	831016	C	8
MNT	-73.900	45.670	18	3.4	104	61	78	831101	A	8
MNT	-74.770	45.700	11	2.8	33	42	67	831210	B	8
MNT	-75.120	45.560	19	3.0	87	51	-8	840117	B	8
MNT	-75.050	45.200	5	3.3	299	41	41	841126	A	8
MNT	-74.240	45.530	11	2.8	107	55	84	860720	C	1
MNT	-74.250	45.100	10	3.3	190	46	76	860813	A	1

MNT	-75.000	45.010	9	3.4	310	40	44	880809	A	3
MNT	-74.990	45.010	9	2.1	314	38	47	880811	A	3
MNT	-75.300	45.210	18	2.9	226	42	-50	900303	C	10
MNT	-74.960	45.580	18	4.1	313	57	53	980418	A	4
PEM	-75.750	45.200	12	4.1	224	22	63	831011	A	8
PEM	-75.750	45.200	12	1.2	52	77	59	831013	B	8
PEM	-76.680	45.610	9	3.1	272	57	66	850824	A	1
PEM	-77.340	45.780	14	3.4	317	48	19	860110	A	1
PEM	-78.420	46.310	4	3.0	178	25	-11	860530	B	1
PEM	-75.630	45.570	7	1.8	348	80	39	870619	C	2
PEM	-75.340	45.770	17	3.5	343	56	78	871111	B	2
PEM	-75.620	45.170	18	3.3	291	46	77	880515	B	3
ECA	-78.930	46.840	13	4.7	320	33	99	000101	A	19
ECA	-95.620	71.180	18	4.1	148	47	65	000405	D	4
ECA	-79.460	43.790	18	3.1	16	25	52	000524	C	4
ECA	-71.070	47.560	18	4.2	289	47	70	000712	B	4
ECA	-113.200		80.570	18	4.6	64	64	16	001003	D
4										
ECA	-116.480		80.940	18	5.2	68	55	30	001113	D
4										
ECA	-63.350	50.030	18	4.2	272	45	86	010324	B	20
ECA	-73.730	44.530	10	5.0	196	40	111	020420	A	19
ECA	-56.000	44.690	20	7.1	122	74	140	291118	A	14
ECA	-56.000	44.690	20	6.8	249	59	166	291118	A	14
ECA	-79.070	46.780	10	6.1	130	45	80	351101	A	16
ECA	-74.100	45.170	9	3.1	300	67	46	760713	B	8
ECA	-68.620	49.840	2	0.0	128	71	69	761000	A	1
ECA	-74.110	46.320	0	4.1	343	42	85	780218	A	6
ECA	-67.330	44.900	12	3.5	255	47	69	840119	B	2
ECA	-70.690	45.370	8	3.5	178	41	75	850412	A	1
ECA	-59.610	57.220	18	4.8	186	56	19	860420	A	3
ECA	-75.560	44.660	2	2.9	195	45	83	870705	B	2
ECA	-79.460	43.470	18	3.4	284	76	-74	870723	D	2
ECA	-78.890	46.850	18	3.2	284	63	72	870817	C	2
ECA	-56.330	56.720	18	4.6	222	53	56	871214	B	3
ECA	-70.820	47.030	14	3.1	296	51	77	880512	A	3
ECA	-71.200	48.130	29	4.7	343	48	82	881123	B	3
ECA	-71.210	48.130	29	6.5	326	67	55	881125	A	3
ECA	-71.180	48.120	29	5.8	170	41	139	881125	B	19
ECA	-71.300	48.140	26	4.1	339	46	103	881126	A	3
ECA	-70.100	60.050	18	5.7	260	42	58	890316	A	3
ECA	-72.640	45.920	18	2.8	66	72	64	900424	C	10
ECA	-71.170	82.180	18	4.7	80	45	-45	950308	A	4
ECA	-71.100	82.220	18	4.0	100	64	-44	950310	C	4
ECA	-59.550	61.000	18	4.2	74	80	-39	950718	C	4
ECA	-106.180		77.100	18	4.6	215	87	35	950824	B
4										
ECA	-107.180		76.670	18	4.7	71	61	29	960222	B
4										
ECA	-87.750	56.670	18	4.0	28	43	-35	960516	C	4
ECA	-76.640	59.610	18	4.2	238	49	80	970714	B	4
ECA	-71.420	46.800	22	4.5	244	35	106	971106	A	19
ECA	-88.190	64.840	18	5.7	216	73	15	971206	A	4
ECA	-54.740	59.090	18	4.9	140	43	1	980121	D	4
ECA	-91.540	76.330	18	4.1	185	53	40	980311	C	4
ECA	-56.380	43.750	18	4.4	215	40	11	980317	D	4
ECA	-79.440	81.900	18	4.3	12	74	-37	980414	B	4
ECA	-60.940	57.830	18	4.0	90	54	-20	980521	C	4
ECA	-89.890	80.970	18	5.3	137	50	2	980609	C	4
ECA	-110.240		79.790	18	5.3	85	48	19	990101	B
4										
ECA	-58.030	60.900	18	5.3	117	41	-12	990729	D	4
ECA	-78.990	43.710	18	3.8	120	61	-28	991126	B	4

ECA	-120.440	75.380	18	5.7	149	77	38	991207	B	4
ECA	-70.010	73.070	10	7.3	172	82	6	331120a	A	15
ECA	-70.010	73.070	10	7.0	190	30	62	331120b	A	15
ECA	-73.600	60.120	3	5.3	251	54	46	891225a	A	12
ECA	-73.600	60.120	3	6.2	240	58	90	891225b	A	12
ECA	-73.600	60.120	3	6.3	200	85	20	891225c	A	12
CVN	-78.100	37.770	10	4.3	66	34	141	031209	A	38
CVN	-78.070	37.750	5	3.6	3	71	158	030505	U	35
CVN	-77.770	38.070	5	0.9	341	41	139	800804	C	37
CVN	-77.770	38.070	3	1.0	310	84	8	800926	C	37
CVN	-77.820	37.890	5	0.3	346	79	136	820118	C	37
CVN	-77.580	37.860	10	2.1	158	61	-8	820605	B	37
CVN	-77.500	37.840	13	1.9	316	42	129	820625	B	37
CVN	-77.500	37.840	13	1.6	327	79	17	820920	B	37
CVN	-78.420	37.750	10	1.9	333	45	-5	830810	C	37
CVN	-78.320	37.870	8	4.0	335	59	16	840817	A	37
CVN	-77.510	37.940	15	1.1	3	63	14	841017	B	37
CVN	-78.440	37.720	7	3.4	346	67	117	810211a	B	37
CVN	-78.400	37.750	10	3.2	278	35	81	810211b	C	37
WVN	-80.540	37.430	18	0.4	340	85	-178	801202	C	37
WVN	-80.510	37.390	16	1.8	340	90	145	830125	A	37
WVN	-80.320	37.510	9	2.2	82	86	-60	830526	B	37
WVN	-80.760	37.270	7	1.0	20	82	-174	830710	C	37
WVN	-80.790	37.200	12	1.1	303	76	27	830912	B	37
WVN	-80.720	37.290	11	1.4	207	66	-147	840207	B	37
NMA	-88.990	36.890	5	4.0	165	85	15	030606	C	35
NMA	-89.680	36.730	2	3.5	175	55	70	040615	B	35
NMA	-90.230	35.750	14	4.1	55	80	-165	050210	A	35
NMA	-90.150	35.830	8	4.2	315	60	20	050501	B	35
NMA	-89.460	36.140	15	3.9	155	65	70	050602	B	35
NMA	-88.960	36.950	4	3.6	320	80	15	050620	A	35
NMA	-89.510	36.370	8	4.2	350	84	145	620202	A	29
NMA	-90.050	36.640	15	4.7	304	78	-28	630303	B	28
NMA	-89.310	37.220	2	3.6	280	70	-20	650814	B	29
NMA	-89.950	35.860	16	4.1	220	75	150	701117	A	29
NMA	-89.680	36.540	9	3.7	85	60	-20	750613	A	29
NMA	-90.480	35.590	16	4.2	45	80	-150	760325	A	29
NMA	-90.480	35.590	12	4.6	220	65	150	760325	A	29
NMA	-89.580	37.160	15	4.3	140	75	50	900926	B	28
NMA	-89.830	36.560	8	4.1	90	67.5	20	910504	A	28
NMA	-89.190	37.360	16	3.9	30	70	170	940205	A	28
NMA	-90.000	35.970	11	3.8	120	65	-15	961129	A	35
NMA	-89.160	36.860	5	3.5	140	70	20	040716a	B	35
ETN	-84.160	35.550	14	3.4	90	53	-16	830708	C	36
ETN	-83.710	36.120	11	3.6	83	80	-2	840214	B	36
ETN	-84.030	35.840	2	3.0	93	85	-29	840317	C	36
ETN	-85.510	35.200	27	3.0	268	40	-26	840419	B	36
ETN	-84.350	35.560	17	3.2	284	56	23	840830	A	36
ETN	-85.210	34.760	18	4.0	90	41	-11	841009	B	36
ETN	-83.710	35.700	13	3.3	63	79	-44	851222	A	36
ETN	-84.750	35.610	22	3.1	254	76	-32	860107	A	36
ETN	-84.500	35.450	19	2.5	256	85	-70	860602	A	36
ETN	-84.990	34.940	13	3.8	109	85	-30	860711	B	36
ETN	-84.190	36.340	13	2.8	283	51	8	870222	C	36
ETN	-84.230	35.570	19	4.2	275	83	45	870327	A	36
ETN	-84.230	35.570	18	2.7	92	80	-18	870409	B	36
ETN	-83.820	36.100	25	3.7	307	55	-4	870711	B	36
ETN	-83.820	36.110	23	3.2	302	59	-16	870711	B	36
ETN	-84.400	35.520	20	3.1	268	41	-12	870901	B	36

ETN	-84.320	35.630	20	3.3	96	71	-30	870922	B	36
ETN	-84.190	35.280	13	2.9	300	62	-22	880109	B	36
ETN	-84.670	35.360	10	2.5	59	48	-19	880213	C	36
ETN	-83.820	35.330	1	3.5	332	50	23	880218	B	36
ETN	-83.990	35.820	14	2.4	290	83	-19	880311	C	36
ETN	-84.210	35.780	18	2.3	261	55	-30	880423	B	36
ETN	-83.740	36.110	17	2.3	111	79	-49	880424	A	36
ETN	-84.430	35.500	23	2.9	266	73	-58	890907	B	36
ETN	-83.930	36.610	25	2.4	113	71	-36	891202	B	36
ETN	-85.020	35.050	4	3.1	227	76	-27	930115	B	36
CHL	-80.178	32.963	7	2.3	300	70	19	810319	B	39
CHL	-80.167	32.935	7	3.3	321	78	52	831106	B	39
CHL	-80.146	32.941	5	1.9	357	49	121	871006	B	39
CHL	-80.148	32.934	6	3.3	276	35	36	880123	A	39
CHL	-80.218	32.979	10	2.0	7	49	119	880623	C	39
CHL	-80.158	32.929	7	2.0	325	40	90	890602	A	39
CHL	-80.155	32.930	7	1.6	350	90	175	890608	A	39
CHL	-80.152	32.949	5	2.8	13	52	161	900618	B	39
CHL	-80.140	32.932	6	2.7	347	77	113	900818	C	39
CHL	-80.130	32.945	4	3.4	10	56	110	901113	C	39
CHL	-80.152	32.987	6	1.5	15	45	115	910824	B	39
EUS	-78.900	46.870	10	4.6	116	68	69	000101	U	25
EUS	-74.250	43.950	6	3.6	150	54	120	000420	U	25
EUS	-80.830	41.990	5	3.9	5	79	159	010126	U	25
EUS	-92.190	35.190	5	4.3	20	85	-165	010504	U	35
EUS	-104.640		37.150	3	4.2	215	30	-80	010904	U 35
EUS	-104.470		37.140	2	4.4	190	25	-130	010905	U 35
EUS	-73.660	44.510	10	5.0	360	35	80	020420	U	35
EUS	-87.780	37.970	19	4.5	120	80	10	020618	U	35
EUS	-98.900	42.810	8	4.1	90	50	-110	021103	U	35
EUS	-80.070	32.360	9	4.0	350	40	90	021111	U	35
EUS	-85.500	34.550	12	4.6	275	75	5	030429	U	35
EUS	-85.500	34.550	12	4.6	275	75	5	030429	U	35
EUS	-101.750		43.100	15	3.9	85	60	-130	030525	U

```
35
EUS     -91.720 36.800  5       3.7     25      80      -165    030816  U       35
EUS     -104.990        36.850  4       4.1     170     55      -100    030913  U
35
EUS     -104.850        36.850  4       4.4     175     55      -95     040322  U
35
EUS     -104.560        32.530  3       3.9     345     50      -120    040523  U
35
EUS     -104.580        32.530  2       3.6     5       70      -110    040622  U
35
EUS     -88.960 41.440  7       4.2     20      90      -165    040628  U       35
EUS     -104.920        36.890  4       4.3     155     65      -120    040801  U
35
EUS     -78.250 43.690  3       3.2     125     65      35      040804  U       35
EUS     -86.280 64.760  23      4.2     155     60      80      040826  U       35
EUS     -85.750 39.610  13      3.8     320     75      15      040912  U       35
EUS     -87.900 32.970  3       4.3     35      40      -115    041107  U       35
EUS     -69.730 47.750  12      4.6     350     30      80      050306  U       35
EUS     -104.860        36.950  4       4.9     160     40      -110    050810  U
35
EUS     -82.800 35.880  8       3.7     90      60      -60     050825  U       35
EUS     -104.570        32.520  5       4.1     230     40      -85     051219  U
35
EUS     -70.460 47.380  25      3.8     15      55      85      060407  U       35
EUS     -68.790 47.000  17      3.5     170     25      45      060714  U       35
EUS     -68.170 44.330  2       3.9     340     35      85      061003  U       35
EUS     -104.900        37.060  2       4.4     205     50      -60     070103  U
35
EUS     -96.270 22.020  11      5.6     190     75      -160    070523  U       35
EUS     -104.790        36.930  4       3.4     195     50      -60     070609  U
35
EUS     -90.940 37.480  5       4.6     260     40      -70     651021  A       29
EUS     -78.200 42.800  2       4.3     110     70      20      660101  A       29
EUS     -104.800        39.900  4       4.5     165     52      -174    670410  U
22
EUS     -78.200 42.900  3       4.1     130     50      40      670613  A       29
EUS     -90.440 37.440  15      4.0     350     60      135     670721  B       28
EUS     -104.700        39.900  3       4.8     130     35      -90     670809  U
22
EUS     -104.700        40.000  5       4.5     158     52      -63     671127  U
22
EUS     -88.370 37.910  22      5.3     0       46      79      681109  A       29
EUS     -86.500 64.400  12      4.6     162     72      90      711002  A       29
EUS     -80.580 33.310  2       4.4     260     40      10      720203  U       24
EUS     -82.530 33.910  2       4.0     350     65      100     720802  U       24
EUS     -89.400 41.600  13      4.1     170     70      160     720915  B       29
EUS     -70.900 45.300  6       4.5     300     80      70      730615  A       29
EUS     -84.000 35.800  13      4.1     190     70      150     731130  C       29
EUS     -88.070 38.550  15      4.3     310     70      0       740403  B       29
EUS     -96.000 45.700  8       4.3     330     90      160     750709  B       29
EUS     -100.700        33.000  3       4.5     260     60      -60     780616  U
28
EUS     -83.910 38.170  12      5.0     30      60      180     800727  U       23
EUS     -66.650 46.980  7       5.1     200     60      125     820111  U       21
EUS     -71.600 43.500  8       4.2     200     35      120     820119  U       21
EUS     -92.210 35.170  6       5.0     330     60      55      820121  U       21
EUS     -74.260 43.940  9       4.9     170     70      115     831007  U       21
EUS     -105.720        42.370  25      5.3     350     60      335     841018  U
21
EUS     -81.160 41.650  6       4.7     25      80      165     860131  U       21
EUS     -84.390 40.550  4       4.4     20      80      -170    860712  U       30
EUS     -87.950 38.710  10      5.0     135     70      15      870610  U       31
EUS     -75.590 46.470  11      4.6     141     42      90      901019  U       25
```

```
EUS     -73.460 45.200  12      3.9     144     45      96      931116  U       25
EUS     -103.300        30.260  20      5.6     114     64      -101    950414  U
26
EUS     -71.910 44.290  6       3.7     95      50      40      950616  U       25
EUS     -74.430 45.990  6       3.7     136     36      98      960314  U       25
EUS     -71.350 44.180  7       3.4     144     60      93      960821  U       25
EUS     -74.190 45.810  22      3.6     96      33      60      970524  U       25
EUS     -87.300 31.200  5       4.9     94      62      -90     971024  U       35
EUS     -69.910 47.670  5       4.3     27      66      111     971028  U       25
EUS     -71.350 46.750  12      4.5     39      63      87      971106  U       25
EUS     -98.510 34.940  19      3.9     120     70      -60     980428  U       35
EUS     -74.720 46.170  9       3.7     150     27      75      980730  U       25
EUS     -80.390 41.490  3       4.5     110     70      20      980925  U       34
EUS     -66.390 49.690  5       4.4     30      63      93      990316  U       25
EUS     -95.560 40.630  12      3.5     290     55      -135    040716b U       35
EUS     -86.930 33.180  4       3.6     30      30      -100    040819b U       35
EUS     -66.660 46.980  9       5.5     200     45      120     820109a U       21
EUS     -66.650 47.020  6       4.8     215     60      130     820109b U       21
EUS     -76.010 40.340  2       4.0     156     45      108     940116a U       25
EUS     -76.010 40.340  3       4.0     121     60      66      940116a U       33
EUS     -76.050 40.340  2       4.6     159     48      102     940116b U       25
EUS     -76.050 40.340  3       4.6     135     49      68      940116b U       33
```

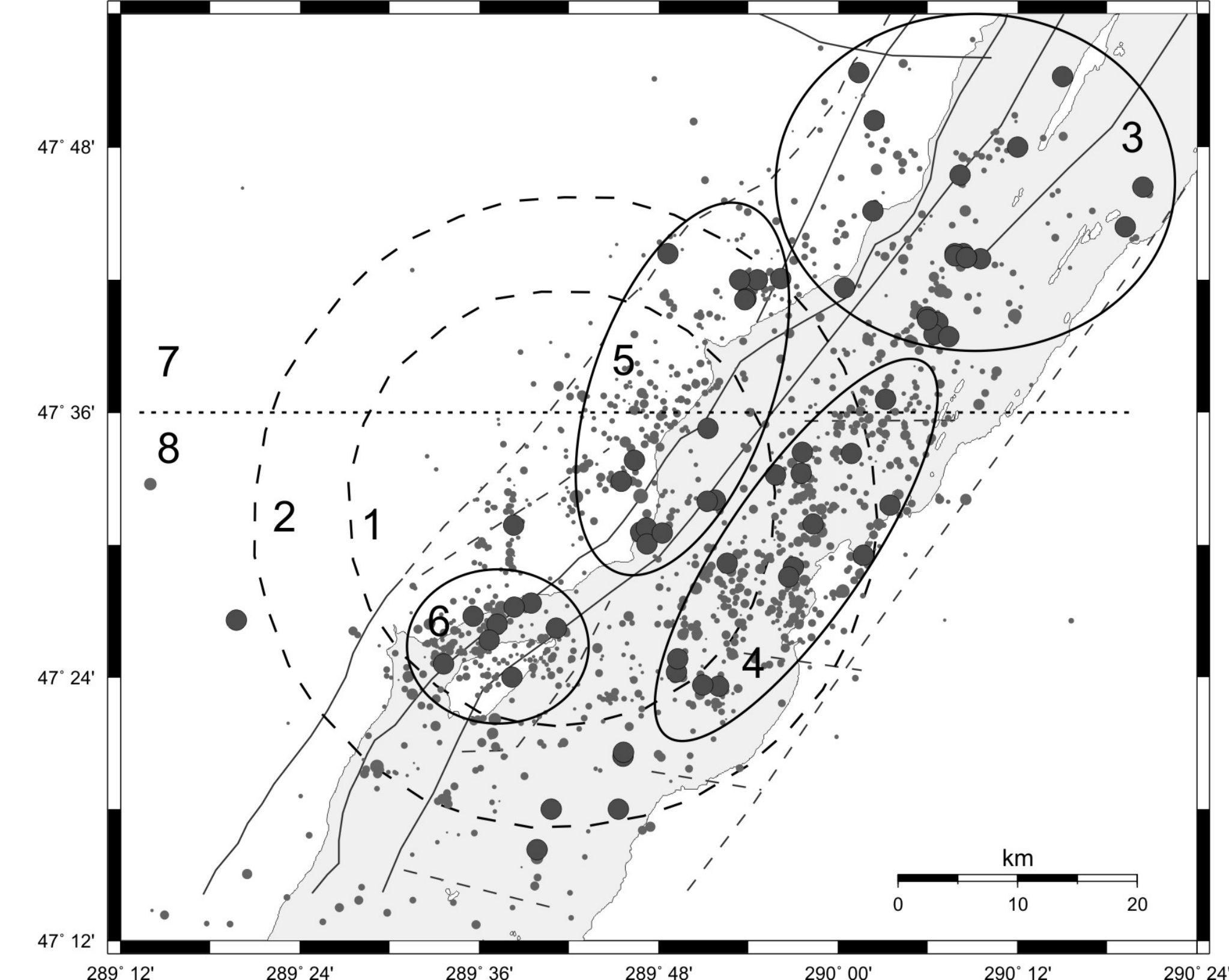
47° 48'
47° 36'
47° 24'
47° 12'
289° 12'
289° 24'
289° 36'
289° 48'
290° 00'
290° 12'
290° 24'
1
2
3
4
5
6
7
8
km
0
10
20

Charlevoix stress field

median 90% CI

Groups with SHmax sub-parallel to local "tectonic" SHmax, about N050
1 - subset below North shore (NW of mid-river splitting line) N046
042 - 050
2 - subset inside small crater (part of 1, except 2 eq) N052
039 - 065
2b - subset central NW (central part of 1) N054
036 - 073

Same but with larger spread or poorer agreement
3 - subset west of E289.85 (S half of 1 + 7 eq) N061
048 - 074
4 - subset ND2 (S part of 1 + 2 eq)
N058 035 - 080
5 - subset ND4 (small cluster below NW shore) N065
045 - 085
5b - subset SW (SW-most part of 1, poorly resolved) N059
041 - 076

Groups with SHmax most oblique to local tectonic stress
6 - subset below east side of river (SE of mid-river line) N103
091 - 115
7 - subset outside large crater (similar to 9) N105
091 - 119
8 - subset depth > 12 km (mostly SE + few NW eq) N116
094 - 139
9 - subset ND1 (N end of CHV, similar to 7) N108
095 - 120

Same but with larger spread or poorer resolution
10 - subset ND3 (but apparently bimodal, poorly resolved ?) N123
105 - 140
11 - subset TD5 (depth 20-23 km, mix spatial distribution) N115
085 - 145
12 - subset Central SE (central part of 2) N111
086 - 136

Conclusions

(1) Events below North shore (NW of mid-river line) show SHmax ~N050, parallel to local tectonic SHmax
possible exceptions:
3 events at NW end that may be part of N-end group (case 9 above)
2 SE events included in ND2 may be part of this group

(2) Groups showing maximum SHmax rotation are North End cluster (ND1, case 9 above), outside large crater
(same as ND1-North End), central SE cluster, and below east side of river at large